

Evaluation of statistical methods for quantifying fractal scaling in water quality time series with irregular sampling

Qian Zhang¹, Ciaran J. Harman², James W. Kirchner^{3,4,5}

¹ University of Maryland Center for Environmental Science at the US Environmental Protection Agency Chesapeake Bay Program Office, 410 Severn Avenue, Suite 112, Annapolis, MD 21403 (formerly, Department of Geography and Environmental Engineering, Johns Hopkins University, 3400 North Charles Street, Baltimore, Maryland 21218)

² Department of Environmental Health and Engineering, Johns Hopkins University, 3400 North Charles Street, Baltimore, Maryland 21218

³ Department of Environmental System Sciences, ETH Zurich, Universitätstrasse 16, CH-8092 Zurich, Switzerland

⁴ Swiss Federal Research Institute WSL, Zürcherstrasse 111, CH-8903 Birmensdorf, Switzerland

⁵ Department of Earth and Planetary Science, University of California, Berkeley, California 94720

Correspondence to: Qian Zhang (qzhang@chesapeakebay.net)

1 **Abstract.** River water-quality time series often exhibit fractal scaling, which here refers to
2 autocorrelation that decays as a power law over some range of scales. Fractal scaling presents
3 challenges to the identification of deterministic trends because (1) fractal scaling has the
4 potential to lead to false inference about the statistical significance of trends and (2) the
5 abundance of irregularly spaced data in water quality monitoring networks complicates efforts to
6 quantify fractal scaling. Traditional methods for estimating fractal scaling -- in the form of
7 spectral slope (β) or other equivalent scaling parameters (*e.g.*, Hurst exponent) -- are generally
8 inapplicable to irregularly sampled data. Here we consider two types of estimation approaches
9 for irregularly sampled data and evaluate their performance using synthetic time series. These
10 time series were generated such that (1) they exhibit a wide range of prescribed fractal scaling
11 behaviors, ranging from white noise ($\beta = 0$) to Brown noise ($\beta = 2$), and (2) their sampling gap
12 intervals mimic the sampling irregularity (as quantified by both the skewness and mean of gap-
13 interval lengths) in real water-quality data. The results suggest that none of the existing methods
14 fully account for the effects of sampling irregularity on β estimation. First, the results illustrate
15 the danger of using interpolation for gap-filling when examining auto-correlation, as the

16 interpolation methods consistently under-estimate or over-estimate β under a wide range of
17 prescribed β values and gap distributions. Second, the widely used Lomb-Scargle spectral
18 method also consistently under-estimates β . A previously published modified form, using only
19 the lowest 5% of the frequencies for spectral slope estimation, has very poor precision, although
20 the overall bias is small. Third, a recent wavelet-based method, coupled with an aliasing filter,
21 generally has the smallest bias and root-mean-squared error among all methods for a wide range
22 of prescribed β values and gap distributions. The aliasing method, however, does not itself
23 account for sampling irregularity, and this introduces some bias in the result. Nonetheless, the
24 wavelet method is recommended for estimating β in irregular time series until improved methods
25 are developed. Finally, all methods' performances depend strongly on the sampling irregularity,
26 highlighting that the accuracy and precision of each method are data-specific. Accurately
27 quantifying the strength of fractal scaling in irregular water-quality time series remains an
28 unresolved challenge for the hydrologic community and for other disciplines that must grapple
29 with irregular sampling.

30 **Key Words**

31 Fractal scaling, autocorrelation, Hurst effect, river water-quality sampling, sampling irregularity,
32 trend analysis

33 **1. Introduction**

34 *1.1. Autocorrelations in Time Series*

35 It is well known that time series from natural systems often exhibit auto-correlation, that is,
36 observations at each time step are correlated with observations one or more time steps in the past.
37 This property is usually characterized by the autocorrelation function (ACF), which is defined as
38 follows for a process X_t at lag k :

$$\gamma(k) = cov(X_t, X_{t+k}) \quad (1)$$

39 In practice, auto-correlation has been frequently modeled with classical techniques such as auto-
40 regressive (AR) or auto-regressive moving-average (ARMA) models (Darken *et al.*, 2002; Yue
41 *et al.*, 2002; Box *et al.*, 2008). These models assume that the underlying process has short-term
42 memory, *i.e.*, the ACF decays exponentially with lag k (Box *et al.*, 2008).

43 Although the short-term memory assumption holds sometimes, it cannot adequately describe
 44 many time series whose ACFs decay as a power law (thus much slower than exponentially) and
 45 may not reach zero even for large lags, which implies that the ACF is non-summable. This
 46 property is commonly referred to as long-term memory or fractal scaling, as opposed to short-
 47 term memory (Beran, 2010).

48 Fractal scaling has been increasingly recognized in studies of hydrological time series,
 49 particularly for the common task of trend identification. Such hydrological series include river
 50 flows (Montanari *et al.*, 2000; Khaliq *et al.*, 2008; Khaliq *et al.*, 2009; Ehsanzadeh and
 51 Adamowski, 2010), air and sea temperatures (Fatichi *et al.*, 2009; Lennartz and Bunde, 2009;
 52 Franzke, 2012b; Franzke, 2012a), conservative tracers (Kirchner *et al.*, 2000; Kirchner *et al.*,
 53 2001; Godsey *et al.*, 2010), and non-conservative chemical constituents (Kirchner and Neal,
 54 2013; Aubert *et al.*, 2014). Because for fractal scaling processes the variance of the sample mean
 55 converges to zero much slower than the rate of n^{-1} (n : sample size), the fractal scaling property
 56 must be taken into account to avoid "false positives" (Type I errors) when inferring the statistical
 57 significance of trends (Cohn and Lins, 2005; Fatichi *et al.*, 2009; Ehsanzadeh and Adamowski,
 58 2010; Franzke, 2012a). Unfortunately, as stressed by Cohn and Lins (2005), it is "surprising that
 59 nearly every assessment of trend significance in geophysical variables published during the past
 60 few decades has failed [to do so]", and a similar tendency is evident in the decade following that
 61 statement as well.

62 ***1.2. Overview of Approaches for Quantification of Fractal Scaling***

63 Several equivalent metrics can be used to quantify fractal scaling. Here we provide a review
 64 of the definitions of such processes and several typical modeling approaches, including both
 65 time-domain and frequency-domain techniques, with special attention to their reconciliation. For
 66 a more comprehensive review, readers are referred to Beran *et al.* (2013), Boutahar *et al.* (2007),
 67 and Witt and Malamud (2013).

68 Strictly speaking, X_t is called a stationary long-memory process if the condition

$$\lim_{k \rightarrow \infty} k^\alpha \gamma(k) = C_1 > 0 \quad (2)$$

69 where C_1 is a constant, is satisfied by some $\alpha \in (0,1)$ (Boutahar *et al.*, 2007; Beran *et al.*, 2013).
 70 Equivalently, X_t is a long-memory process if, in the spectral domain, the condition

$$\lim_{\omega \rightarrow 0} |\omega|^\beta f(\omega) = C_2 > 0 \quad (3)$$

71 is satisfied by some $\beta \in (0,1)$, where C_2 is a constant and $f(\omega)$ is the spectral density function
 72 of X_t , which is related to ACF as follows (which is also known as the Wiener-Khinchin theorem):

$$f(\omega) = \frac{1}{2\pi} \sum_{k=-\infty}^{\infty} \gamma(k) e^{-ik\omega} \quad (4)$$

73 where ω is angular frequency (Boutahar *et al.*, 2007).

74 One popular model for describing long-memory processes is the so-called fractional auto-
 75 regressive integrated moving-average model, or ARFIMA (p, q, d) , which is an extension of
 76 ARMA models and is defined as follows:

$$(1 - B)^d \varphi(B) X_t = \psi(B) \varepsilon_t \quad (5)$$

77 where ε_t is a series of independent, identically distributed Gaussian random numbers $\sim (0, \sigma_\varepsilon^2)$,
 78 B is the backshift operator (*i.e.*, $BX_t = X_{t-1}$), and functions $\varphi(\cdot)$ and $\psi(\cdot)$ are polynomials of order
 79 p and q , respectively. The fractional differencing parameter d is related to the parameter α in Eq.
 80 (2) as follows:

$$d = \frac{1 - \alpha}{2} \in (-0.5, 0.5) \quad (6)$$

81 (Beran *et al.*, 2013; Witt and Malamud, 2013).

82 In addition to a slowly decaying ACF, a long-memory process manifests itself in two other
 83 equivalent fashions. One is the so-called ‘‘Hurst effect’’, which states that, on a log-log scale, the
 84 range of variability of a process changes linearly with the length of the time period under
 85 consideration. This power-law slope is often referred to as the ‘‘Hurst exponent’’ or ‘‘Hurst
 86 coefficient’’ H (Hurst, 1951), which is related to d as follows:

$$H = d + 0.5 \quad (7)$$

87 (Beran *et al.*, 2013; Witt and Malamud, 2013). The second equivalent description of long-
 88 memory processes, this time from a frequency-domain perspective, is ‘‘fractal scaling’’, which
 89 describes a power-law decrease in spectral power with increasing frequency, yielding power
 90 spectra that are linear on log-log axes (Lomb, 1976; Scargle, 1982; Kirchner, 2005).

91 Mathematically, this inverse proportionality can be expressed as:

$$f(\omega) = C_3 |\omega|^{-\beta} \quad (8)$$

92 where C_3 is a constant and the scaling exponent β is termed the ‘‘spectral slope.’’ In particular, for
 93 spectral slopes of zero, one, and two, the underlying processes are termed as ‘‘white’’, ‘‘pink’’ (or

94 “flicker”), and “Brown” (or “red”) noises, respectively (Witt and Malamud, 2013). Illustrative
 95 examples of these three noises are shown in **Figure 1a-1c**.

96 In addition, it can be shown that the spectral density function for ARFIMA (p,d,q) is

$$f(\omega) = \frac{\sigma_\varepsilon^2 |\psi(e^{-i\omega})|^2}{2\pi |\varphi(e^{-i\omega})|^2} |1 - e^{-i\omega}|^{-2d} \quad (9)$$

97 for $-\pi < \omega < \pi$ (Boutahar *et al.*, 2007; Beran *et al.*, 2013). For $|\omega| \ll 1$, Eq. (9) can be
 98 approximated by:

$$f(\omega) = C_4 |\omega|^{-2d} \quad (10)$$

99 with

$$C_4 = \frac{\sigma_\varepsilon^2 |\psi(1)|^2}{2\pi |\varphi(1)|^2} \quad (11)$$

100 Eq. (10) thus exhibits the asymptotic behavior required for a long-memory process given by Eq.
 101 (3). In addition, a comparison of Eq. (10) and (8) reveals that,

$$\beta = 2d \quad (12)$$

102 Overall, these derivations indicate that these different types of scaling parameters (*i.e.*, α , d , and
 103 H and β) can be used equivalently to describe the strength of fractal scaling. Specifically, their
 104 equivalency can be summarized as follows:

$$\beta = 2d = 1 - \alpha = 2H - 1 \quad (13)$$

105 It should be noted, however, that the parameters d , α , and H are only applicable over a fixed
 106 range of fractal scaling, which is equivalent to $(-1, 1)$ in terms of β .

107 ***1.3. Motivation and Objective of this Work***

108 To account for fractal scaling in trend analysis, one must be able to first quantify the strength
 109 of fractal scaling for a given time series. Numerous estimation methods have been developed for
 110 this purpose, including Hurst rescaled range analysis, Higuchi’s method, Geweke and Porter-
 111 Hudak’s method, Whittle’s maximum likelihood estimator, detrended fluctuation analysis, and
 112 others (Taqqu *et al.*, 1995; Montanari *et al.*, 1997; Montanari *et al.*, 1999; Rea *et al.*, 2009;
 113 Stroe-Kunold *et al.*, 2009). For brevity, these methods are not elaborated here; readers are
 114 referred to Beran (2010) and Witt and Malamud (2013) for details. While these estimation
 115 methods have been extensively adopted, they are unfortunately only applicable to regular (*i.e.*,
 116 evenly spaced) data, *e.g.*, daily streamflow discharge, monthly temperature, *etc.* In practice,
 117 many types of hydrological data, including river water-quality data, are often sampled irregularly

118 or have missing values, and hence their strengths of fractal scaling cannot be readily estimated
119 with the above traditional estimation methods.

120 Thus, estimation of fractal scaling in irregularly sampled data is an important challenge for
121 hydrologists and practitioners. Many data analysts may be tempted to interpolate the time series
122 to make it regular and hence analyzable (Graham, 2009). Although technically convenient,
123 interpolation can be problematic if it distorts the series' autocorrelation structure (Kirchner and
124 Weil, 1998). In this regard, it is important to evaluate various types of interpolation methods
125 using carefully designed benchmark tests and to identify the scenarios under which the
126 interpolated data can yield reliable (or, alternatively, biased) estimates of spectral slope.

127 Moreover, quantification of fractal scaling in real-world water-quality data is subject to
128 several common complexities. First, water-quality data are rarely normally distributed; instead,
129 they are typically characterized by log-normal or other skewed distributions (Hirsch *et al.*, 1991;
130 Helsel and Hirsch, 2002), with potential consequences for β estimation. Moreover, water-quality
131 data also tend to exhibit long-term trends, seasonality, and flow-dependence (Hirsch *et al.*, 1991;
132 Helsel and Hirsch, 2002), which can also affect the accuracy of β estimates. Thus, it may be
133 more plausible to quantify β in transformed time series after accounting for the seasonal patterns
134 and discharge-driven variations in the original time series, which is the approach taken in this
135 paper. For the trend aspect, however, it remains a puzzle whether the data set should be de-
136 trended before conducting β estimation. Such de-trending treatment can certainly affect the
137 estimated value of β and hence the validity of (or confidence in) any inference made regarding
138 the statistical significance of temporal trends in the time series. This somewhat circular issue is
139 beyond the scope of our current work -- it has been previously discussed in the context of short-
140 term memory (Zetterqvist, 1991; Darken *et al.*, 2002; Yue *et al.*, 2002; Noguchi *et al.*, 2011;
141 Clarke, 2013; Sang *et al.*, 2014), but it is not well understood in the context of fractal scaling (or
142 long-term memory) and hence presents an important area for future research.

143 In the above context, the main objective of this work was to use Monte Carlo simulation to
144 systematically evaluate and compare two broad types of approaches for estimating the strength
145 of fractal scaling (*i.e.*, spectral slope β) in irregularly sampled river water-quality time series.
146 Specific aims of this work include the following:

147 (1) To examine the sampling irregularity of typical river water-quality monitoring data and
148 to simulate time series that contain such irregularity; and

149 (2) To evaluate two broad types of approaches for estimating β in simulated irregularly
150 sampled time series.

151 The first type of approach includes several forms of interpolation techniques for gap filling, thus
152 making the data regular and analyzable by traditional estimation methods. The second type of
153 approach includes the well-known Lomb-Scargle periodogram (Lomb, 1976; Scargle, 1982) and
154 a recently developed wavelet method combined with a spectral aliasing filter (Kirchner and Neal,
155 2013). The latter two methods can be directly applied to irregularly spaced data; here we aim to
156 compare them with the interpolation techniques. Details of these various approaches are
157 provided in **Section 3.1**.

158 This work was designed to make several specific contributions. First, it uses benchmark tests
159 to quantify the performance of a wide range of methods for estimating fractal scaling in
160 irregularly sampled water-quality data. Second, it proposes an innovative and general approach
161 for modeling sampling irregularity in water-quality records. Third, while this work was not
162 intended to compare all published estimation methods for fractal scaling, it does provide and
163 demonstrate a generalizable framework for data simulation (with gaps) and β estimation, which
164 can be readily applied toward the evaluation of other methods that are not covered here. Last but
165 not least, while this work was intended to help hydrologists and practitioners understand the
166 performance of various approaches for water-quality time series, the findings and approaches
167 may be broadly applicable to irregularly sampled data in other scientific disciplines.

168 The rest of the paper is organized as follows. We propose a general approach for modeling
169 sampling irregularity in typical river water-quality data and discuss our approach for simulating
170 irregularly sampled data (**Section 2**). We then introduce the various methods for estimating
171 fractal scaling in irregular time series and compare their estimation performance (**Section 3**). We
172 close with a discussion of the results and implications (**Section 4**).

173 **2. Quantification of Sampling Irregularity in River Water-Quality Data**

174 ***2.1. Modeling of Sampling Irregularity***

175 River water-quality data are often sampled irregularly. In some cases, samples are taken
176 more frequently during particular periods of interest, such as high flows or drought periods; here
177 we will address the implications of the irregularity, but not the (intentional) bias, inherent in such
178 a sampling strategy. In other cases, the sampling is planned with a fixed sampling interval (*e.g.*,

179 1 day) but samples are missed (or lost, or fail quality-control checks) at some time steps during
180 implementation. In still other cases, the sampling is intrinsically irregular because, for example,
181 one cannot measure the chemistry of rainfall on rainless days or the chemistry of a stream that
182 has dried up. Theoretically, any deviation from fixed-interval sampling can affect the subsequent
183 analysis of the time series.

184 To quantify the sampling irregularity, we propose a simple and general approach that can be
185 applied to any time series of monitoring data. Specifically, for a given time series with N points,
186 the time intervals between adjacent samples are calculated; these intervals themselves make up a
187 time series of $N-1$ points that we call Δt . In addition, the following parameters are calculated to
188 quantify its sampling irregularity:

- 189 • L = the length of the period of record,
- 190 • N = the number of samples in the record,
- 191 • $\Delta t_{nominal}$ = the nominal sampling interval under regular sampling (*e.g.*, $\Delta t_{nominal} = 1$ day
192 for daily samples),
- 193 • $\Delta t^* = \Delta t / \Delta t_{nominal}$, the sample intervals non-dimensionalized by the nominal sampling
194 interval,
- 195 • $\Delta t_{average} = L / (N - 1)$ the average of all the entries in Δt .

196 The quantification is illustrated with two simple examples. The first example contains data
197 sampled every hour from 1:00 am to 11:00 am on one day. In this case, $L = 10$ hours, $N = 11$
198 samples, $\Delta t = \{1, 1, 1, 1, 1, 1, 1, 1, 1, 1\}$ hour, and $\Delta t_{nominal} = \Delta t_{average} = 1$ hour. The second
199 example contains data sampled at 1:00 am, 3:00 am, 4:00 am, 8:00 am, and 11:00 am. In this
200 case, $L = 10$ hours, $N = 5$ samples, $\Delta t = \{2, 1, 4, 3\}$ hours, $\Delta t_{nominal} = 1$ hour, and $\Delta t_{average} = 2.5$
201 hours. It is readily evident that the first case corresponds to fixed-interval (regular) sampling that
202 has the property of $\Delta t_{average} / \Delta t_{nominal} = 1$ (dimensionless), whereas the second case corresponds to
203 irregular sampling for which $\Delta t_{average} / \Delta t_{nominal} > 1$.

204 The dimensionless set Δt^* contains essential information for determining sampling
205 irregularity. This set is modeled as independent, identically distributed values drawn from a
206 negative binomial (NB) distribution. This distribution has two dimensionless parameters, the
207 shape parameter (λ) and the mean parameter (μ), which collectively represent the irregularity of
208 the samples. The NB distribution is a flexible distribution that provides a discrete analogue of a

209 gamma distribution. The geometric distribution, itself the discrete analogue of the exponential
210 distribution, is a special case of the NB distribution when $\lambda = 1$.

211 The parameters μ and λ represent different aspects of sampling irregularity, as illustrated by
212 the examples shown in **Figure 2**. The mean parameter μ represents the fractional increase in the
213 average interval between samples due to gaps: $\mu = \text{mean}(\Delta t^*) - 1 = (\Delta t_{\text{average}} - \Delta t_{\text{nominal}})/\Delta t_{\text{nominal}}$.
214 Thus the special case of $\mu = 0$ corresponds to regular sampling (*i.e.*, $\Delta t_{\text{average}} = \Delta t_{\text{nominal}}$), whereas
215 any larger value of μ corresponds to irregular sampling (*i.e.*, $\Delta t_{\text{average}} > \Delta t_{\text{nominal}}$) (**Figure 2c**). The
216 shape parameter λ characterizes the similarity of gaps to each other; that is, a small λ indicates
217 that the samples contain gaps of widely varying lengths, whereas a large λ indicates that the
218 samples contain many gaps of similar lengths (**Figure 2a-2b**).

219 To visually illustrate these gap distributions, representative samples of irregular time series
220 are presented in **Figure 1** for the three special processes described above (**Section 1.2**), *i.e.*,
221 white noise, pink noise, and Brown noise. Specifically, three different gap distributions, namely,
222 $\text{NB}(\lambda = 1, \mu = 1)$, $\text{NB}(\lambda = 1, \mu = 14)$, and $\text{NB}(\lambda = 0.01, \mu = 1)$, were simulated and each was
223 applied to convert the three original (regular) time series (**Figure 1a-1c**) to irregular time series
224 (**Figure 1d-1f**). These simulations clearly illustrate the effects of the two parameters λ and μ . In
225 particular, compared with $\text{NB}(\lambda = 1, \mu = 1)$, $\text{NB}(\lambda = 1, \mu = 14)$ shows a similar level of sampling
226 irregularity (same λ) but a much longer average gap interval (larger μ). Again compared with
227 $\text{NB}(\lambda = 1, \mu = 1)$, $\text{NB}(\lambda = 0.01, \mu = 1)$ shows the same average interval (same μ) but a much more
228 irregular (skewed) gap distribution that contains a few very large gaps (smaller λ).

229 **2.2. Examination of Sampling Irregularity in Real River Water-Quality Data**

230 The above modeling approach was applied to real water-quality data from two large river
231 monitoring networks in the United States to examine sampling irregularity. One such network is
232 the Chesapeake Bay River Input Monitoring program, which typically samples streams bi-
233 monthly to monthly, accompanied with additional sampling during stormflows (Langland *et al.*,
234 2012; Zhang *et al.*, 2015). These data were obtained from the U.S. Geological Survey National
235 Water Information System (<http://doi.org/10.5066/F7P55KJN>). The other network is the Lake
236 Erie and Ohio tributary monitoring program, which typically samples streams at a daily
237 resolution (National Center for Water Quality Research, 2015). For each site, we determined the
238 NB parameters to quantify sampling irregularity. The mean parameter μ can be estimated as
239 described above, and the shape parameter λ can be calculated directly from the mean and

240 variance of Δt^* as follows: $\lambda = \mu^2 / [\text{var}(\Delta t^*) - \mu] = (\text{mean}(\Delta t^*) - 1)^2 / [\text{var}(\Delta t^*) - \text{mean}(\Delta t^*) + 1]$.
241 Alternatively, a maximum likelihood approach can be used, which employs the “*fitdist*” function
242 in the “*fitdistrplus*” R package (Delignette-Muller and Dutang, 2015). In general, the two
243 approaches produce similar results, which are summarized in **Table 1**, with two examples of
244 fitted NB distributions shown in **Figure 3**.

245 For the Chesapeake Bay River Input Monitoring program (9 sites), total nitrogen (TN) and
246 total phosphorus (TP) are taken as representatives of water-quality constituents. According to the
247 maximum likelihood approach, the shape parameter λ varies between 0.7 and 1.2 for TN and
248 between 0.8 and 1.1 for TP (**Table 1**). These λ values are around 1.0, reflecting the fact that
249 these sites have relatively even gap distributions (*i.e.*, relatively balanced counts of large and
250 small gaps). The mean parameter μ varies between 9.5 and 19.6 for TN and between 13.4 and
251 24.4 for TP in the Chesapeake monitoring network, corresponding to $\Delta t_{\text{average}}$ of 10.5–20.6 days
252 for TN and 14.4–25.4 days for TP, respectively. This is consistent with the fact that these sites
253 have typically been sampled bi-monthly to monthly, along with additional sampling during
254 stormflows (Langland *et al.*, 2012; Zhang *et al.*, 2015).

255 For the Lake Erie and Ohio tributary monitoring program (6 sites), records of nitrate-plus-
256 nitrite (NO_x) and TP were examined. According to the maximum likelihood approach, the shape
257 parameter λ is approximately 0.01 for both constituents (**Table 1**). These very low λ values occur
258 because these time series contain a few very large gaps, ranging from 35 days to 1109 days (~3
259 years). The mean parameter μ varies between 0.06 and 0.22, corresponding to $\Delta t_{\text{average}}$ of 1.06
260 and 1.22 days, respectively. This is consistent with fact that these sites have been sampled at a
261 daily resolution with occasional missing values on some days (Zhang and Ball, 2017).

262 **2.3. Simulation of Time Series with Irregular Sampling**

263 To evaluate the various β estimation methods, our first step was to use Monte Carlo
264 simulation to produce time series that mimic the sampling irregularity observed in real water-
265 quality monitoring data. We began by simulating regular (gap free) time series using the
266 fractional noise simulation method of Witt and Malamud (2013), which is based on inverse
267 Fourier filtering of white noises. Our analysis showed this method performed reasonably well
268 compared to other simulation methods for β values between 0 and 1 (see Supporting Information
269 S1). In addition, this method can also simulate β values beyond this range. The noises simulated
270 by the Witt and Malamud method, however, are band-limited to the Nyquist frequency (half of

271 the sampling frequency) of the underlying white noise time series, whereas true fractional noises
272 would contain spectral power at all frequencies, extending well above the Nyquist frequency for
273 any sampling. Thus these band-limited noises will be less susceptible to spectral aliasing than
274 true fractional noises would be; see Kirchner (2005) for detailed discussions of the aliasing issue.

275 100 replicates of regular (gap free) time series were produced for nine prescribed spectral
276 slopes, which vary from $\beta = 0$ (white noise) to $\beta = 2$ (Brownian motion or “random walk”) with
277 an increment of 0.25 (*i.e.*, 0, 0.25, 0.5, 0.75, 1.0, 1.25, 1.5, 1.75, and 2). These regular time series
278 each have a length (N) of 9125, which can be interpreted as 25 years of regular daily samples
279 (that is, $\Delta t_{nominal} = 1$ day).

280 The simulated regular time series were converted to irregular time series using gap intervals
281 that were simulated with NB distributions. To make these gap intervals mimic those in typical
282 river water-quality time series, representative NB parameters were chosen based on results from
283 **Section 2.2**. Specifically, μ was set at 1 and 14, corresponding to $\Delta t_{average}$ of 2 days and 15 days
284 respectively. For λ , we chose four values that span three orders of magnitude, *i.e.*, 0.001, 0.1, 1,
285 and 10. Note that when $\lambda = 1$ the generated time series corresponds to a Bernoulli process. With
286 the chosen values of μ and λ , a total of eight scenarios were generated, which were implemented
287 using the “*rnbinom*” function in the “*stats*” R package (R Development Core Team, 2014):

- 288 1) $\mu = 1$ (*i.e.*, $\Delta t_{average} / \Delta t_{nominal} = 2$), $\lambda = 0.01$,
- 289 2) $\mu = 1$, $\lambda = 0.1$,
- 290 3) $\mu = 1$, $\lambda = 1$,
- 291 4) $\mu = 1$, $\lambda = 10$,
- 292 5) $\mu = 14$ (*i.e.*, $\Delta t_{average} / \Delta t_{nominal} = 15$), $\lambda = 0.01$,
- 293 6) $\mu = 14$, $\lambda = 0.1$,
- 294 7) $\mu = 14$, $\lambda = 1$,
- 295 8) $\mu = 14$, $\lambda = 10$.

296 Examples of these simulations are shown with boxplots in **Figure 2**.

297 3. Evaluation of Proposed Estimation Methods for Irregular Time Series

298 3.1. Summary of Estimation Methods

299 For the simulated irregular time series, β was estimated using the aforementioned two types
300 of approaches. The first type includes 11 different interpolation methods (designated as B1-B11
301 below) to fill the data gaps, thus making the data regular and analyzable by traditional methods:

- 302 B1) Global mean: all missing values replaced with the mean of all observations;
- 303 B2) Global median: all missing values replaced with the median of all observations;
- 304 B3) Random replacement: all missing values replaced with observations randomly drawn
305 (with replacement) from the time series;
- 306 B4) Next observation carried backward: each missing value replaced with the next available
307 observation;
- 308 B5) Last observation carried forward: each missing value replaced with the preceding
309 available observation;
- 310 B6) Average of the two nearest samples: each missing value replaced with the mean of its
311 next and preceding available observations;
- 312 B7) Lowess (locally weighted scatterplot smoothing) with a smoothing span of 1: missing
313 values replaced using fitted values from a lowess model determined using all available
314 observations (Cleveland, 1981);
- 315 B8) Lowess with a smoothing span of 0.75: same as B7 except that the smoothing span is 75%
316 of the available data (similar distinction follows for B9-B11);
- 317 B9) Lowess with a smoothing span of 50%;
- 318 B10) Lowess with a smoothing span of 30%; and
- 319 B11) Lowess with a smoothing span of 10%.

320 B4 and B5 were implemented using the “*na.locf*” function in the “*zoo*” R package (Zeileis and
321 Grothendieck, 2005). B7-B11 were implemented using the “*loess*” function in the “*stats*” R
322 package (R Development Core Team, 2014). An illustration of these interpolation methods is
323 provided in **Figure 4**. The interpolated data, along with the original regular data (designated as
324 A1) were analyzed using the Whittle’s maximum likelihood method for β estimation, which was
325 implemented using the “*FDWhittle*” function in the “*fractal*” R package (Constantine and
326 Percival, 2014).

327 The second type of approaches estimates β directly from the irregularly sampled data, using
328 several variants of the Lomb-Scargle periodogram (designated as C1a-C1c below), and a
329 recently developed wavelet-based method (designated as C2 below). Specifically, these
330 approaches are:

331 C1a) Lomb-Scargle periodogram: the spectral density of the time series (with gaps) is
332 estimated and the spectral slope is fit using all frequencies (Lomb, 1976; Scargle, 1982).
333 This is a classic method for examining periodicity in irregularly sampled data, which is
334 analogous to the more familiar fast Fourier transform method often used for regularly
335 sampled data;

336 C1b) Lomb-Scargle periodogram with 5% data: same as C1a except that the fitting of the
337 spectral slope considers only the lowest 5% of the frequencies (Montanari *et al.*, 1999);

338 C1c) Lomb-Scargle periodogram with “binned” data: same as C1a except that the fitting of
339 the spectral slope is performed on binned data in three steps: (1) The entire range of
340 frequency is divided into 100 equal-interval bins on logarithmic scale. (2) The
341 respective medians of frequency and power spectral density are calculated for each of
342 the 100 bins. (3) The 100 pairs of median frequency and median spectral density are
343 used to estimate the spectral slope on a log-log scale.

344 C2) Kirchner and Neal (2013)’s wavelet method: uses a modified version of Foster’s
345 weighted wavelet spectrum (Foster, 1996) to suppress spectral leakage from low
346 frequencies and applies an aliasing filter (Kirchner, 2005) to remove spectral aliasing
347 artifacts at high frequencies.

348 C1a was implemented using the “*spec.ls*” function in the “*cts*” R package (Wang, 2013). C2 was
349 run in *C*, using codes modified from those in Kirchner and Neal (2013).

350 **3.2. Evaluation of Methods’ Performance**

351 Each estimation method listed above was applied to the simulated data (**Section 2.3**) to
352 estimate β , which were then compared with the prescribed (“true”) β to quantify the performance
353 of each method. Plots of method evaluation for all simulations are provided as **Figures S3-S12**
354 (Supporting Information S2). Close inspections of these plots reveal some general patterns of the
355 methods’ performance. For brevity, these patterns are presented with a subset of the plots, which
356 correspond to the cases where true $\beta = 1$ and shape parameter $\lambda = 0.01, 0.1, 1, \text{ and } 10$ (**Figure 5**).
357 In general, β values estimated using the regular data (A1) are very close to 1.0, which indicates

358 that the adopted fractional noise generation method and the Whittle's maximum likelihood
359 estimator have small combined simulation and estimation bias. This is perhaps unsurprising,
360 since the estimator is based on the Fourier transform and the noise generator is based on an
361 inverse Fourier transform; thus, one method is essentially just the inverse of the other. One
362 should also note that when fractional noises are not arbitrarily band-limited at the Nyquist
363 frequency (as they inherently are with the noise generator that is used here), spectral aliasing
364 should lead to spectral slopes that are flatter than expected (Kirchner, 2005), and thus to
365 underestimates of LRD.

366 For the simulated irregular data, the estimation methods differ widely in their performance.
367 Specifically, three interpolation methods (*i.e.*, B4-B6) consistently over-estimate β , indicating
368 that they introduce additional correlations into the time series, reducing its short-timescale
369 variability. In contrast, the other eight interpolation methods (*i.e.*, B1-B3 and B7-B11) generally
370 under-estimate β , indicating that the interpolated points are less correlated than the original time
371 series, thus introducing additional variability on short timescales. As expected, results from the
372 lowess methods (B7-B11) depend strongly on the size of smoothing window, that is, β is more
373 severely under-estimated as the smoothing window becomes wider. In fact, when the smoothing
374 window is 1.0 (*i.e.*, method B7), lowess performs the interpolation using all data available and
375 thus behaves similarly to interpolations based on global means (B1) or global medians (B2),
376 except that lowess fits a polynomial curve instead of constant values. However, whenever a
377 sampling gap is much shorter than the smoothing window, the infilled lowess value will be close
378 to the local mean or median, and the abrupt jumps produced by these infilled values will
379 artificially increase the variance in the time series at high frequencies, leading to an artificially
380 reduced spectral slope β and correspondingly, an underestimate of β . This mechanism explains
381 why lowess interpolation distorts β more when there are many small gaps (large λ), and therefore
382 more jumps to, and away from, the infilled values, than when there are only a few large gaps
383 (small λ).

384 Among the direct methods (*i.e.*, C1a, C1b, C1c, and C2), the Lomb-Scargle method, with
385 original data (C1a) or binned data (C1c) tends to under-estimate β , though the underestimation
386 by C1c is generally less severe. The modified Lomb-Scargle method (C1b), using only the
387 lowest 5% of frequencies, yields estimates that are centered around 1.0. However, C1b has the
388 highest variability (*i.e.*, least precision) in β estimates among all methods. Compared with all the

389 above methods, the wavelet method (C2) has much better performance in terms of both accuracy
 390 and precision when λ is 1 or 10, a slightly better performance when λ is 0.1, but worse
 391 performance when λ is 0.01.

392 The shape parameter λ greatly affects the performance of the estimation methods. All the
 393 interpolation methods that under-estimate β (*i.e.*, B1-B3 and B7-B11) perform worse as λ
 394 increases from 0.01 to 10. This effect can be interpreted as follows: when the time series
 395 contains a large number of relatively small gaps (*e.g.*, $\lambda = 1$ or 10), there are many jumps (which,
 396 as noted above, contain mostly high-frequency variance) between the original data and the
 397 infilled values, resulting in more severe under-estimation. In contrast, when the data contain only
 398 a small number of very large gaps (*e.g.*, $\lambda = 0.01$ or 0.1), there are fewer of these jumps, resulting
 399 in minimal under-estimation. Similar effects of λ are also observed with the interpolation
 400 methods that show over-estimation (*i.e.*, B4-B6) – that is, over-estimation is more severe when λ
 401 is larger. Similarly, the Lomb-Scargle method (C1a and C1c) performs worse (more serious
 402 underestimation) as λ increases. Finally, method C2 seems to perform the best when λ is large (1
 403 or 10), but not well when λ is very small (0.01), as noted above. This result highlights the
 404 sensitivity of the wavelet method to the presence of a few large gaps in the time series. For such
 405 cases, a potentially more feasible approach is to break the whole time series into several
 406 segments (each without long gaps) and then apply the wavelet method (C2) to analyze each
 407 segment separately. If this can yield more accurate estimates, then further simulation
 408 experiments should be designed to systematically determine how long the gap needs to be to
 409 invoke such an approach.

410 Next, the method evaluation is extended to all the simulated spectral slopes, that is, $\beta = 0$,
 411 0.25, 0.5, 0.75, 1.0, 1.25, 1.5, 1.75, and 2. For ease of discussion, three quantitative criteria were
 412 proposed for evaluating performance, namely, bias (B), standard deviation (SD), and root-mean-
 413 squared error (RMSE), as defined below:

$$B_i = \bar{\beta}_i - \beta_{true} \quad (14)$$

$$SD_i = \sqrt{\frac{1}{99} \sum_{j=1}^{100} (\beta_{i,j} - \bar{\beta}_i)^2} \quad (15)$$

$$RMSE_i = \sqrt{B_i^2 + SD_i^2} \quad (16)$$

414 where $\bar{\beta}_i$ is the mean of 100 β values estimated by method i , and β_{true} is the prescribed β value
415 for simulation of the initial regular time series. In general, B and SD can be considered as the
416 models' systematic error and random error, respectively, and RMSE serves as an integrated
417 measure of both errors. For all evaluations, plots of bias and RMSE are provided in the main text.
418 (Plots of SD are provided as **Figure S7** and **Figure S12** for simulations with $\mu = 1$ and $\mu = 14$,
419 respectively.)

420 For simulations with $\mu = 1$, results of estimation bias and RMSE are summarized in **Figure 6**
421 and **Figure 7**, respectively. (More details are provided in **Figures S3-S6**.) For brevity, we focus
422 on three direct methods (C1a, C1b and C2) and three representative interpolation methods.
423 (Specifically, B1 represents B1-B3 and B7; B6 represents B4-B6, and B8 represents B8-B11.)
424 Overall, these six methods show mixed performances. In terms of bias (**Figure 6**), B1 (global
425 mean) and B8 (lowess with a smoothing span of 0.75) tend to have negative bias, particularly for
426 time series with (1) moderate-to-large β_{true} values and (2) large λ values (*i.e.*, less skewed gap
427 intervals). By contrast, B1 and B8 generally have minimal bias when (1) β_{true} is close to zero (*i.e.*,
428 when the simulated time series is close to white noise); and (2) λ is small (*e.g.*, 0.01), since
429 interpolating a few large gaps cannot significantly affect the overall correlation structure. In
430 addition, lowess interpolation with a larger smoothing window tends to yield more negatively
431 biased estimates (data not shown). The other interpolation method, B6 (mean of the two nearest
432 neighbors) tends to over-estimate β , particularly for time series with (1) small β_{true} values and (2)
433 large λ values. At large β_{true} values (*e.g.*, 2.0), the auto-correlation is already very strong such
434 that taking the mean of two neighbors for gap filling does not introduce much additional
435 correlation, as opposed to the case of small β_{true} values. The Lomb-Scargle methods (C1a and
436 C1b) generally have negative bias, particularly for time series with (1) moderate-to-large β_{true}
437 values (for both methods) and (2) large λ values (for C1a), which is similar to B1 and B8.
438 However, C1b overall shows less severe bias than C1a. Finally, the wavelet method (C2) shows
439 generally the smallest bias among all methods. However, its performance advantage is not as
440 great when the time series has small λ values (*i.e.*, very skewed gap intervals), as noted above,
441 which may be due to the fact that the aliasing filter was designed for regular time series. In terms
442 of SD (**Figure S7**), method C1b performs the worst among all methods (as noted above), method
443 B6 and B8 perform poorly for large β_{true} values, and method C2 performs poorly for $\beta_{true} = 0$. In
444 terms of RMSE (**Figure 7**), methods B1, B8, C1a, and C1b perform well for small β_{true} values

445 and small λ values, whereas method B6 performs well for large β_{true} values and small λ values. In
 446 comparison, method C2 has the smallest RMSEs among all methods, and its RMSEs are
 447 similarly small for the wide range of β_{true} and λ values. In general, the wavelet method can be
 448 considered the best among all the tested methods.

449 For simulations with $\mu = 14$, results of estimation bias and RMSE are summarized in
 450 **Figure 8** and **Figure 9**, respectively. (More details are provided in **Figures S8-S11**.) Overall,
 451 these methods show mixed performances that are generally similar to the cases when $\mu = 1$, as
 452 discussed above. These results highlight the generality of these methods' performances, which
 453 applies at least to the range of $\mu = [1, 14]$. In addition, all methods show generally larger RMSE
 454 for $\mu = 14$ than $\mu = 1$, indicating their dependence on the mean gap interval (**Figure 9**). Perhaps
 455 the most notable difference is observed with method C2, which in this case shows positive bias
 456 for small λ values (0.01 and 0.1) and negative bias for large λ values (1 and 10) (**Figure 8f**). It
 457 nonetheless generally shows the smallest RMSEs among all the tested methods.

458 **3.3. Quantification of Spectral Slopes in Real Water-Quality Data**

459 In this section, the proposed estimation approaches were applied to quantify β in real water-
 460 quality data from the two monitoring programs presented in **Section 2.2** (**Table 1**). As noted in
 461 **Section 1.3**, such real data are typically much more complex than our simulated time series,
 462 because of (1) strong deviations from normal distributions and (2) effects of flow-dependence,
 463 seasonality, and temporal trends (Hirsch *et al.*, 1991; Helsel and Hirsch, 2002). In this regard,
 464 future research may simulate time series with these important characteristics and evaluate the
 465 performance of various estimation approaches, perhaps following the modeling framework
 466 described here. Alternatively, one may quantify β in transformed time series after accounting for
 467 the above aspects. In this work, we have taken the latter approach for a preliminary investigation.
 468 Specifically, we have used the published Weighted Regressions on Time, Discharge, and Season
 469 (WRTDS) method (Hirsch *et al.*, 2010) to transform the original time series. This widely
 470 accepted method estimates daily concentrations based on discretely collected concentration
 471 samples using time, season, and discharge as explanatory variables, *i.e.*,

$$471 \quad \ln(C) = \beta_0 + \beta_1 t + \beta_2 \ln(Q) + \beta_3 \sin(2\pi t) + \beta_4 \cos(2\pi t) + \varepsilon \quad (17)$$

472 where C is concentration, Q is daily discharge, t is time in decimal years, β_i are fitted
 473 coefficients, and ε is the error term. The 2nd and 3rd terms on the right represent time and
 474 discharge effects, respectively, whereas the 4th and 5th terms collectively represent cyclical

475 seasonal effects. For a full description of this method, see Hirsch *et al.* (2010). In this work,
476 WRTDS was applied to obtain time series of estimated daily concentrations for each constituent
477 at each site. The difference between observed concentration (C_{obs}) and estimated concentration
478 (C_{est}) was calculated in logarithmic space to obtain the concentration residuals,

$$residuals = \ln(C_{obs}) - \ln(C_{est}) \quad (18)$$

479 For our data sets, histograms of concentration residuals (expressed in natural log concentration
480 units) are shown in **Figures S13-S16** (Supporting Information S3). Compared with the original
481 concentration data, these model residuals are much more nearly normal and homoscedastic.
482 Moreover, the model residuals are less susceptible to the issues of temporal, seasonal, and
483 discharge-driven variations than the original concentrations. Therefore, the model residuals are
484 more appropriate than the original concentrations for β estimation using the simulation
485 framework adopted in this work.

486 The estimated β values for the concentration residuals are summarized in **Figure 10**. Clearly,
487 the estimated β varies considerably with the estimation method. In addition, the estimated β
488 varies with site and constituent (*i.e.*, TP, TN, or NO_x .) Our discussion below focuses on the
489 wavelet method (C2), because it is established above that this method performs better than the
490 other estimation methods under a wide range of gap conditions. We emphasize that it is beyond
491 our current scope to precisely quantify β in these water-quality data sets, but our simulation
492 results presented above (**Section 3.2**) can be used as references to qualitatively evaluate the
493 reliability of C2 and/or other methods for these data sets.

494 For TN and TP concentration data at the Chesapeake River Input Monitoring sites (**Table 1**),
495 μ varies between 9.5 and 24.4, whereas λ is ~ 1.0 . Thus, the simulated gap scenario of NB($\mu = 14$,
496 $\lambda = 1$) can be used as a reasonable reference to assess methods' reliability (**Figure 8**). Based on
497 method C2, the estimated β ranges between $\beta = 0.36$ and $\beta = 0.61$ for TN and between $\beta = 0.30$
498 and $\beta = 0.58$ for TP at these sites (**Figure 10**). For such ranges, the simulation results indicate
499 that method C2 tends to moderately under-estimate β under this gap scenario (**Figure 8**), and
500 hence spectral slopes for TN and TP at these Chesapeake sites are probably slightly higher than
501 those presented above.

502 For NO_x and TP concentration data at the Lake Erie and Ohio sites (**Table 1**), μ varies
503 between 0.06 and 0.22, whereas λ is ~ 0.01 . Thus, the simulated gap scenario of NB($\mu = 1$, $\lambda =$
504 0.01) can be used as a reasonable reference to assess the methods' reliability (**Figure 6**). For

505 such small λ (*i.e.*, a few gaps that are very dissimilar from others), C2 is not reliable for β
506 estimation, as reflected by the generally positive bias in the simulation results. By contrast,
507 methods B1 (interpolation with global mean) and B8 (lowess with span 0.75) both perform quite
508 well under this gap scenario (**Figure 6**). These two methods provide almost identical β estimates
509 for each site-constituent combination, ranging from $\beta = 1.0$ to $\beta = 1.5$ for NO_x and from $\beta = 1.0$
510 to $\beta = 1.4$ for TP (**Figure 10**).

511 Overall, the above analysis of real water-quality data has illustrated the wide variability in β
512 estimates, with different choices of estimation methods yielding very different results. To our
513 knowledge, these water-quality data have not previously been analyzed in this context. As
514 illustrated above, our simulation experiments (**Section 3.2**) can be used as references to coarsely
515 evaluate the reliability of each method under specific gap scenarios, thereby considerably
516 narrowing the likely range of the estimated spectral slopes. Nonetheless, our results demonstrate
517 that the analyzed water-quality time series can exhibit strong fractal scaling, particularly at the
518 Lake Erie and Ohio tributary sites. Thus, an important implication is that researchers and
519 analysts should be cautious when applying standard statistical methods to identify temporal
520 trends in such water-quality data sets (Kirchner and Neal, 2013). In future work, one may
521 consider applying Bayesian statistical analysis or other approaches to more accurately quantify
522 the spectral slope and associated uncertainty for real water-quality data analysis. In addition, the
523 modeling framework presented here (including both gap simulation and β estimation) may be
524 extended to simulations of irregular time series that have prescribed spectral slopes and also
525 superimposed temporal trends, which can then be used to evaluate the validity of various
526 statistical methods for identifying trends and their associated statistical significance.

527 **4. Conclusions**

528 River water-quality time series often exhibit fractal scaling behavior, which presents
529 challenges to the identification of deterministic trends. Because traditional spectral estimation
530 methods are generally not applicable to irregularly sampled time series, we have examined two
531 broad types of estimation approaches and evaluated their performances against synthetic data
532 with a wide range of prescribed β values and gap intervals that are representative of the sampling
533 irregularity of real water-quality data.

534 The results of this work suggest several important messages. First, the results remind us of
535 the risks in using interpolation for gap filling when examining auto-correlation, as the
536 interpolation methods consistently under-estimate or over-estimate β under a wide range of
537 prescribed β values and gap distributions. Second, the widely used Lomb-Scargle spectral
538 method also consistently under-estimates β . Its modified form, using the 5% lowest frequencies
539 for spectral slope estimation, has very poor precision, although the overall bias is small. Third,
540 the wavelet method, coupled with an aliasing filter, has the smallest bias and root-mean-squared
541 error among all methods for a wide range of prescribed β values and gap distributions, except for
542 cases with small prescribed β values (*i.e.*, close to white noise) or small λ values (*i.e.*, very
543 skewed gap distributions). Thus, the wavelet method is recommended for estimating spectral
544 slopes in irregular time series until improved methods are developed. In this regard, future
545 research should aim to develop an aliasing filter that is more applicable to irregular time series
546 with very skewed gap intervals. Finally, all methods' performances depend strongly on the
547 sampling irregularity in terms of both the skewness and mean of gap-interval lengths,
548 highlighting that the accuracy and precision of each method are data-specific.

549 Overall, these results provide new contributions in terms of better understanding and
550 quantification of the proposed methods' performances for estimating the strength of fractal
551 scaling in irregularly sampled water-quality data. In addition, the work has provided an
552 innovative and general approach for modeling sampling irregularity in water-quality records.
553 Moreover, this work has proposed and demonstrated a generalizable framework for data
554 simulation (with gaps) and β estimation, which can be readily applied to evaluate other methods
555 that are not covered in this work. More generally, the findings and approaches may also be
556 broadly applicable to irregularly sampled data in other scientific disciplines. Last but not least,
557 we note that accurate quantification of fractal scaling in irregular water-quality time series
558 remains an unresolved challenge for the hydrologic community and for many other disciplines
559 that must grapple with irregular sampling.

560 **Data Availability**

561 River monitoring data used in this study are available through the U.S. Geological Survey
562 National Water Information System (<http://doi.org/10.5066/F7P55KJN>) and the Heidelberg
563 University's National Center for Water Quality Research.

564 **Supporting Information**

565 Supporting information to this article is available online.

566 **Competing Interests**

567 The authors declare that they have no conflict of interest.

568 **Acknowledgements**

569 Zhang was supported by the Maryland Sea Grant through awards NA10OAR4170072 and
570 NA14OAR1470090 and by the Maryland Water Resources Research Center through a graduate
571 fellowship while he was a doctoral student at the Johns Hopkins University. Subsequent support to Zhang
572 was provided by the USEPA under grant “EPA/CBP Technical Support 2017” (No. 07-5-230480).
573 Harman’s contribution to this work was supported by the National Science Foundation through grants
574 CBET-1360415 and EAR-1344664. We thank Bill Ball (Johns Hopkins University) and Bob Hirsch (U.S.
575 Geological Survey) for many useful discussions. This is contribution no. 5449 of the University of
576 Maryland Center for Environmental Science.

577 **References**

- 578 Aubert, A. H., J. W. Kirchner, C. Gascuel-Oudou, M. Fauchoux, G. Gruau and P. Mérot, 2014. Fractal
579 water quality fluctuations spanning the periodic table in an intensively farmed watershed.
580 *Environ. Sci. Technol.* 48:930-937, DOI: 10.1021/es403723r.
- 581 Beran, J., 2010. Long-range dependence. *Wiley Interdiscip. Rev. Comput. Stat.* 2:26-35, DOI:
582 10.1002/wics.52.
- 583 Beran, J., Y. Feng, S. Ghosh and R. Kulik, 2013. *Long-Memory Processes: Probabilistic Properties and*
584 *Statistical Methods*. Berlin, Heidelberg, Springer Berlin Heidelberg, ISBN 978-3-642-35511-0
- 585 Boutahar, M., V. Marimoutou and L. Nourira, 2007. Estimation Methods of the Long Memory Parameter:
586 Monte Carlo Analysis and Application. *J. Appl. Stat.* 34:261-301, DOI:
587 10.1080/02664760601004874.
- 588 Box, G. E. P., G. M. Jenkins and G. C. Reinsel, 2008. *Time Series Analysis, Fourth Edition*. Hoboken, NJ,
589 John Wiley & Sons, Inc., ISBN 9781118619193
- 590 Clarke, R. T., 2013. Calculating uncertainty in regional estimates of trend in streamflow with both serial
591 and spatial correlations. *Water Resour. Res.* 49:7120-7125, DOI: 10.1002/wrcr.20465.
- 592 Cleveland, W. S., 1981. LOWESS: A program for smoothing scatterplots by robust locally weighted

593 regression. *Am. Stat.* 35:54, DOI: 10.2307/2683591.

594 Cohn, T. A. and H. F. Lins, 2005. Nature's style: Naturally trendy. *Geophys. Res. Lett.* 32:L23402, DOI:
595 10.1029/2005GL024476.

596 Constantine, W. and D. Percival, 2014. *fractal: Fractal Time Series Modeling and Analysis*,

597 Darken, P. F., C. E. Zipper, G. I. Holtzman and E. P. Smith, 2002. Serial correlation in water quality
598 variables: Estimation and implications for trend analysis. *Water Resour. Res.* 38:1117, DOI:
599 10.1029/2001WR001065.

600 Delignette-Muller, M. L. and C. Dutang, 2015. fitdistrplus: An R Package for Fitting Distributions. *J.*
601 *Stat. Softw.* 64:1-34, DOI.

602 Ehsanzadeh, E. and K. Adamowski, 2010. Trends in timing of low stream flows in Canada: impact of
603 autocorrelation and long-term persistence. *Hydrol. Process.* 24:970-980, DOI: 10.1002/hyp.7533.

604 Fatichi, S., S. M. Barbosa, E. Caporali and M. E. Silva, 2009. Deterministic versus stochastic trends:
605 Detection and challenges. *J. Geophys. Res.* 114:D18121, DOI: 10.1029/2009JD011960.

606 Foster, G., 1996. Wavelets for period analysis of unevenly sampled time series. *Astron. J.* 112:1709-1729,
607 DOI, <http://articles.adsabs.harvard.edu/full/1996AJ....112.1709F>.

608 Franzke, C., 2012a. Nonlinear Trends, Long-Range Dependence, and Climate Noise Properties of Surface
609 Temperature. *J. Clim.* 25:4172-4183, DOI: 10.1175/JCLI-D-11-00293.1.

610 Franzke, C., 2012b. On the statistical significance of surface air temperature trends in the Eurasian Arctic
611 region. *Geophys. Res. Lett.* 39:L23705, DOI: 10.1029/2012GL054244.

612 Godsey, S. E., W. Aas, T. A. Clair, H. A. de Wit, I. J. Fernandez, J. S. Kahl, I. A. Malcolm, C. Neal, M.
613 Neal, S. J. Nelson, S. A. Norton, M. C. Palucis, B. L. Skjelkvåle, C. Soulsby, D. Tetzlaff and J. W.
614 Kirchner, 2010. Generality of fractal 1/f scaling in catchment tracer time series, and its
615 implications for catchment travel time distributions. *Hydrol. Process.* 24:1660-1671, DOI:
616 10.1002/hyp.7677.

617 Graham, J., 2009. Missing Data Analysis: Making It Work in the Real World. *Annu. Rev. Psychol.* 60:549-
618 576, DOI: 10.1146/annurev.psych.58.110405.085530.

619 Helsel, D. R. and R. M. Hirsch, 2002. Statistical Methods in Water Resources. *U.S. Geological Survey*
620 *Techniques of Water-Resources Investigations Book 4, Chapter A3*. U.S. Geological Survey,
621 Reston, VA, p. 522. <http://pubs.usgs.gov/twri/twri4a3/>.

622 Hirsch, R. M., R. B. Alexander and R. A. Smith, 1991. Selection of methods for the detection and
623 estimation of trends in water quality. *Water Resour. Res.* 27:803-813, DOI: 10.1029/91WR00259.

624

625 Hirsch, R.M., D.L. Moyer and S.A. Archfield, 2010. Weighted regressions on time, discharge, and season
626 (WRTDS), with an application to Chesapeake Bay river inputs. *J. Am. Water Resour. Assoc.*

627 46:857-880, DOI: 10.1111/j.1752-1688.2010.00482.x.

628 Hurst, H. E., 1951. Long-term storage capacity of reservoirs. *Trans. Amer. Soc. Civil Eng.* 116:770-808,
629 DOI.

630 Khaliq, M. N., T. B. M. J. Ouarda and P. Gachon, 2009. Identification of temporal trends in annual and
631 seasonal low flows occurring in Canadian rivers: The effect of short- and long-term persistence.
632 *J. Hydro.* 369:183-197, DOI: 10.1016/j.jhydrol.2009.02.045.

633 Khaliq, M. N., T. B. M. J. Ouarda, P. Gachon and L. Sushama, 2008. Temporal evolution of low-flow
634 regimes in Canadian rivers. *Water Resour. Res.* 44:W08436, DOI: 10.1029/2007WR006132.

635 Kirchner, J., 2005. Aliasing in $1/f^\alpha$ noise spectra: Origins, consequences, and remedies. *Phys. Rev. E*
636 71:066110-066110, DOI: 10.1103/PhysRevE.71.066110.

637 Kirchner, J. W., X. Feng and C. Neal, 2000. Fractal stream chemistry and its implications for contaminant
638 transport in catchments. *Nature* 403:524-527, DOI: 10.1038/35000537.

639 Kirchner, J. W., X. Feng and C. Neal, 2001. Catchment-scale advection and dispersion as a mechanism
640 for fractal scaling in stream tracer concentrations. *J. Hydro.* 254:82-101, DOI: 10.1016/s0022-
641 1694(01)00487-5.

642 Kirchner, J. W. and C. Neal, 2013. Universal fractal scaling in stream chemistry and its implications for
643 solute transport and water quality trend detection. *Proc. Natl. Acad. Sci. U. S. A.* 110:12213-
644 12218, DOI: 10.1073/pnas.1304328110.

645 Kirchner, J. W. and A. Weil, 1998. No fractals in fossil extinction statistics. *Nature* 395:337-338, DOI:
646 10.1038/26384.

647 Langland, M. J., J. D. Blomquist, D. L. Moyer and K. E. Hyer, 2012. Nutrient and suspended-sediment
648 trends, loads, and yields and development of an indicator of streamwater quality at nontidal sites
649 in the Chesapeake Bay watershed, 1985-2010. U.S. Geological Survey Scientific Investigations
650 Report 2012-5093, Reston, VA, p. 26. <http://pubs.usgs.gov/sir/2012/5093/pdf/sir2012-5093.pdf>.

651 Lennartz, S. and A. Bunde, 2009. Trend evaluation in records with long-term memory: Application to
652 global warming. *Geophys. Res. Lett.* 36:L16706, DOI: 10.1029/2009GL039516.

653 Lomb, N. R., 1976. Least-squares frequency analysis of unequally spaced data. *Astrophysics and Space*
654 *Science* 39:447-462, DOI: 10.1007/BF00648343.

655 Montanari, A., R. Rosso and M. S. Taquq, 1997. Fractionally differenced ARIMA models applied to
656 hydrologic time series: Identification, estimation, and simulation. *Water Resour. Res.* 33:1035-
657 1044, DOI: 10.1029/97WR00043.

658 Montanari, A., R. Rosso and M. S. Taquq, 2000. A seasonal fractional ARIMA Model applied to the Nile
659 River monthly flows at Aswan. *Water Resour. Res.* 36:1249-1259, DOI:
660 10.1029/2000WR900012.

661 Montanari, A., M. S. Taqqu and V. Teverovsky, 1999. Estimating long-range dependence in the presence
662 of periodicity: An empirical study. *Math. Comput. Model.* 29:217-228, DOI: 10.1016/S0895-
663 7177(99)00104-1.

664 National Center for Water Quality Research, 2015. Tributary Data Download. Accessed July 23, 2015,
665 [https://www.heidelberg.edu/academics/research-and-centers/national-center-for-water-quality-](https://www.heidelberg.edu/academics/research-and-centers/national-center-for-water-quality-research/tributary-data-download)
666 [research/tributary-data-download](https://www.heidelberg.edu/academics/research-and-centers/national-center-for-water-quality-research/tributary-data-download).

667 Noguchi, K., Y. R. Gel and C. R. Duguay, 2011. Bootstrap-based tests for trends in hydrological time
668 series, with application to ice phenology data. *J. Hydro.* 410:150-161, DOI:
669 10.1016/j.jhydrol.2011.09.008.

670 R Development Core Team, 2014. R: A language and environment for statistical computing. R Foundation
671 for Statistical Computing, Vienna, Austria. ISBN 3900051070. <http://www.r-project.org>.

672 Rea, W., L. Oxley, M. Reale and J. Brown, 2009. Estimators for Long Range Dependence: An Empirical
673 Study. *Electron. J. Stat.*, <http://arxiv.org/abs/0901.0762>, DOI.

674 Sang, Y.-F., Z. Wang and C. Liu, 2014. Comparison of the MK test and EMD method for trend
675 identification in hydrological time series. *J. Hydro.* 510:293-298, DOI:
676 10.1016/j.jhydrol.2013.12.039.

677 Scargle, J. D., 1982. Studies in Astronomical Time-Series Analysis. II. Statistical Aspects of Spectral-
678 Analysis of Unevenly Spaced Data. *Astrophys. J.* 263:835-853, DOI: 10.1086/160554.

679 Stroe-Kunold, E., T. Stadnytska, J. Werner and S. Braun, 2009. Estimating long-range dependence in time
680 series: an evaluation of estimators implemented in R. *Behav. Res. Methods* 41:909-923, DOI:
681 10.3758/BRM.41.3.909.

682 Taqqu, M. S., V. Teverovsky and W. Willinger, 1995. Estimators for long-range dependence: an empirical
683 study. *Fractals*, <http://www.worldscientific.com/doi/abs/10.1142/S0218348X95000692>, DOI.

684 Wang, Z., 2013. cts: An R Package for Continuous Time Autoregressive Models via Kalman Filter. *J.*
685 *Stat. Softw.* 53:1-19, DOI.

686 Witt, A. and B. D. Malamud, 2013. Quantification of Long-Range Persistence in Geophysical Time
687 Series: Conventional and Benchmark-Based Improvement Techniques. *Surv. Geophys.* 34:541-
688 651, DOI: 10.1007/s10712-012-9217-8.

689 Yue, S., P. Pilon, B. Phinney and G. Cavadias, 2002. The influence of autocorrelation on the ability to
690 detect trend in hydrological series. *Hydrol. Process.* 16:1807-1829, DOI: 10.1002/hyp.1095.

691 Zeileis, A. and G. Grothendieck, 2005. zoo: S3 Infrastructure for Regular and Irregular Time Series. *J.*
692 *Stat. Softw.* 14:1-27, DOI.

693 Zetterqvist, L., 1991. Statistical Estimation and Interpretation of Trends in Water Quality Time Series.
694 *Water Resour. Res.* 27:1637-1648, DOI: 10.1029/91wr00478.

695 Zhang, Q. and W. P. Ball, 2017. Improving Riverine Constituent Concentration and Flux Estimation by
696 Accounting for Antecedent Discharge Conditions. *J. Hydro.* 547:387–402, DOI:
697 10.1016/j.jhydrol.2016.12.052.

698 Zhang, Q., D. C. Brady, W. R. Boynton and W. P. Ball, 2015. Long-Term Trends of Nutrients and
699 Sediment from the Nontidal Chesapeake Watershed: An Assessment of Progress by River and
700 Season. *J. Am. Water Resour. Assoc.* 51:1534-1555, DOI: 10.1111/1752-1688.12327.

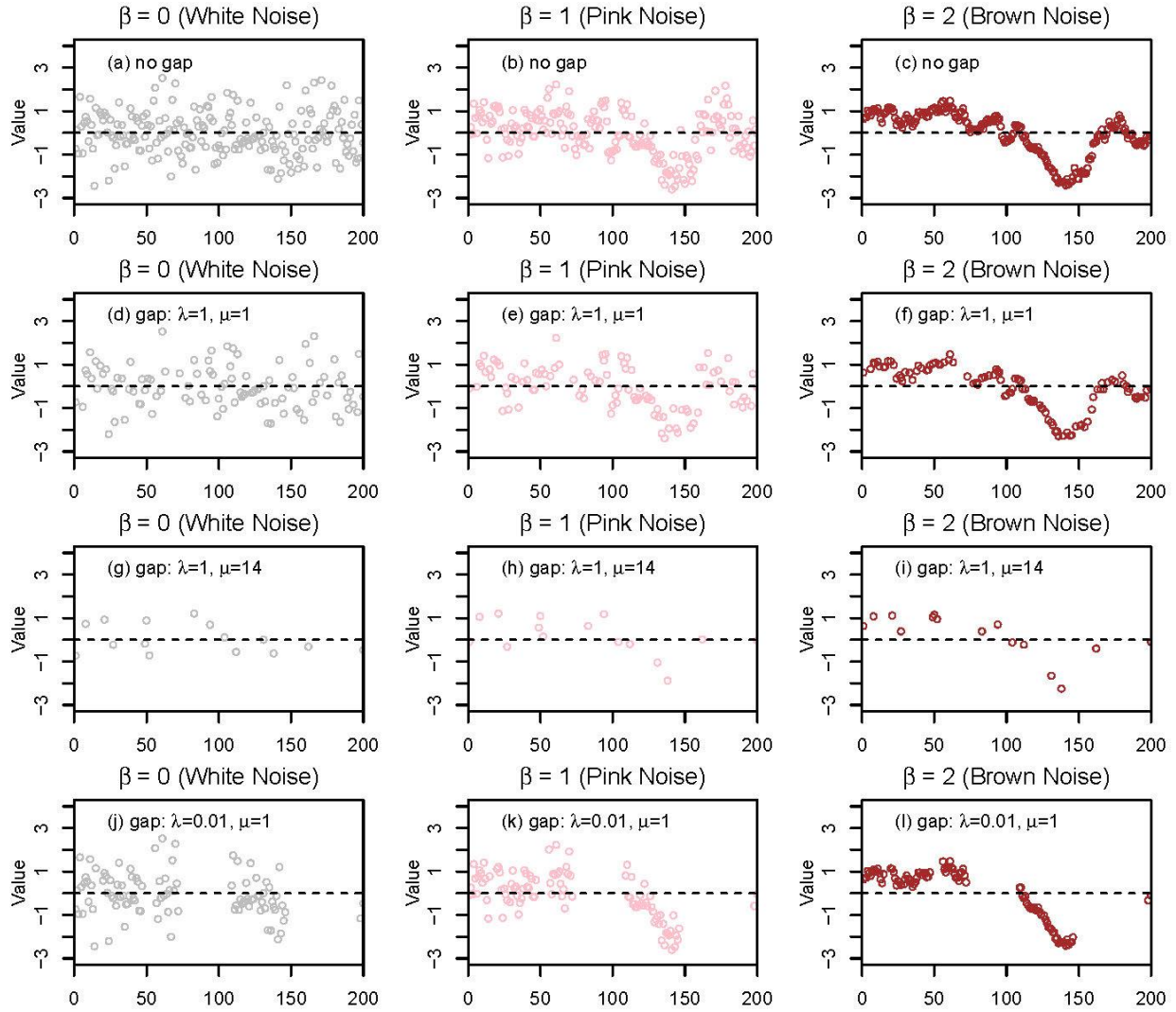
Table 1. Quantification of sampling irregularity for selected water-quality constituents at nine sites of the Chesapeake Bay River Input Monitoring program and six sites of the Lake Erie and Ohio tributary monitoring program. (μ : mean parameter; λ : shape parameter estimated using maximum likelihood; λ' : shape parameter estimated using the direct approach (see **Section 2.2**). $\Delta t_{average}$: average gap interval; N : total number of samples.)

I. Chesapeake Bay River Input Monitoring program

Site ID	River and station name	Drainage area (mi ²)	Total nitrogen (TN)					Total phosphorus (TP)				
			λ	λ'	μ	$\Delta t_{average}$ (days)	N	λ	λ'	μ	$\Delta t_{average}$ (days)	N
01578310	Susquehanna River at Conowingo, MD	27,100	0.8	1.1	13.5	14.5	876	0.8	1.0	13.4	14.4	881
01646580	Potomac River at Chain Bridge, Washington D.C.	11,600	0.9	0.6	9.5	10.5	1,385	1.1	1.0	24.4	25.4	579
02035000	James River at Cartersville, VA	6,260	0.8	1.0	13.9	14.9	960	0.8	1.1	13.7	14.7	974
01668000	Rappahannock River near Fredericksburg, VA	1,600	0.8	0.6	15.6	16.6	776	0.8	0.6	15.2	16.2	796
02041650	Appomattox River at Matoaca, VA	1,340	0.8	0.8	15.1	16.1	798	0.8	0.8	14.9	15.9	810
01673000	Pamunkey River near Hanover, VA	1,071	0.8	0.9	15.1	16.1	873	0.8	1.0	14.7	15.7	894
01674500	Mattaponi River near Beulahville, VA	601	0.7	0.9	14.3	15.3	810	0.8	0.9	14.2	15.2	820
01594440	Patuxent River at Bowie, MD	348	0.9	1.1	15.3	16.3	787	0.8	0.8	14.0	15.0	861
01491000	Choptank River near Greensboro, MD	113	1.2	1.5	19.6	20.6	680	1.1	1.0	20.5	21.5	690

II. Lake Erie and Ohio tributary monitoring program

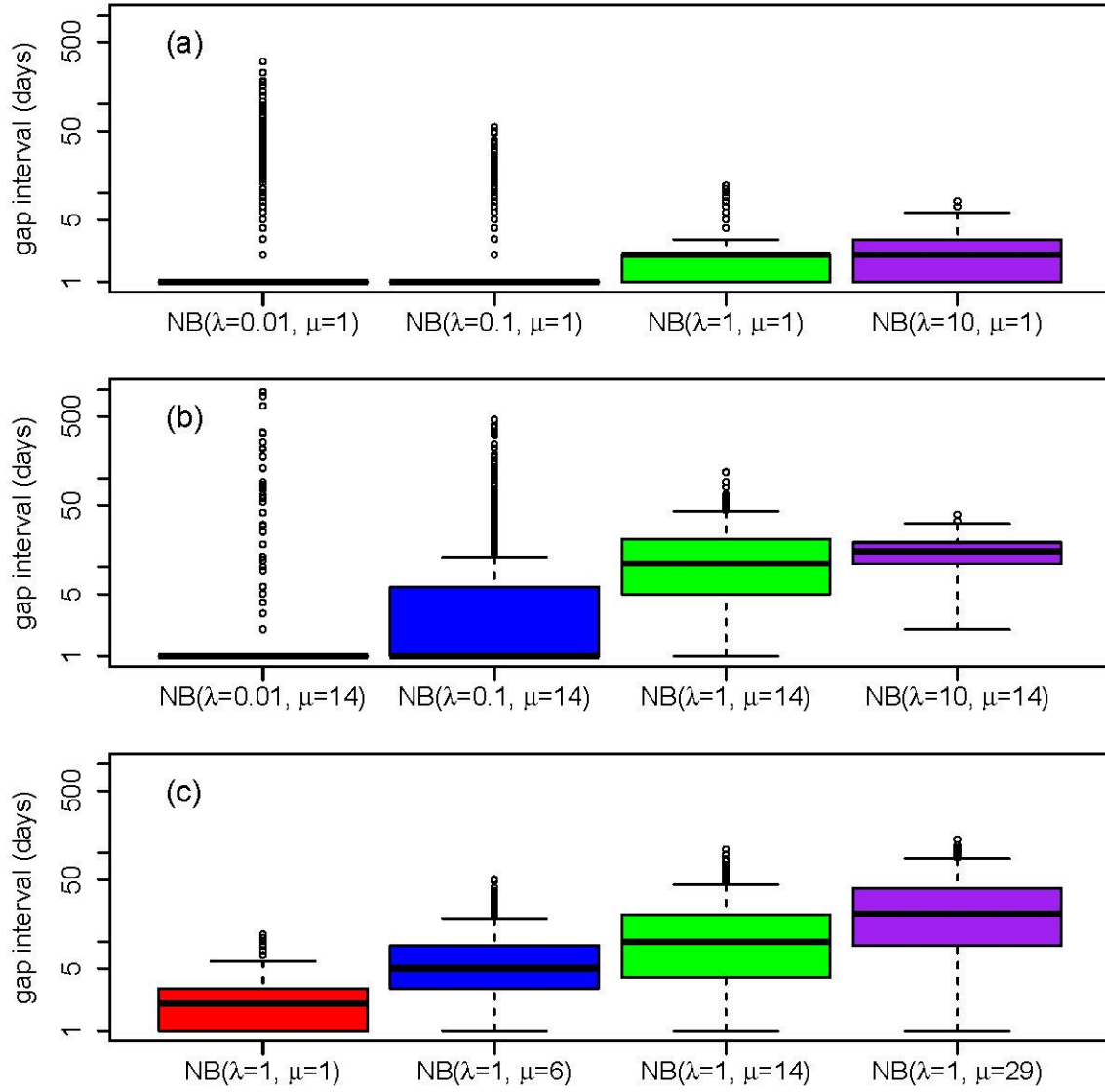
Site ID	River and station name	Drainage area (mi ²)	Nitrate-plus-nitrite (NO _x)					Total phosphorus (TP)				
			λ	λ'	μ	$\Delta t_{average}$ (days)	N	λ	λ'	μ	$\Delta t_{average}$ (days)	N
04193500	Maumee River at Waterville, OH	6,330	0.005	0.0003	0.19	1.19	9,101	0.005	0.0003	0.19	1.19	9,101
04198000	Sandusky River near Fremont, OH	1,253	0.01	0.003	0.22	1.22	9,641	0.01	0.003	0.22	1.22	9,655
04208000	Cuyahoga River at Independence, OH	708	0.007	0.006	0.13	1.13	7,421	0.007	0.006	0.13	1.13	7,426
04212100	Grand River near Painesville, OH	686	0.01	0.005	0.21	1.21	5,023	0.01	0.005	0.22	1.22	4,994
04197100	Honey Creek at Melmore, OH	149	0.007	0.005	0.06	1.06	9,914	0.007	0.005	0.06	1.06	9,914
04197170	Rock Creek at Tiffin, OH	34.6	0.007	0.008	0.06	1.06	8,422	0.007	0.008	0.06	1.06	8,440



701

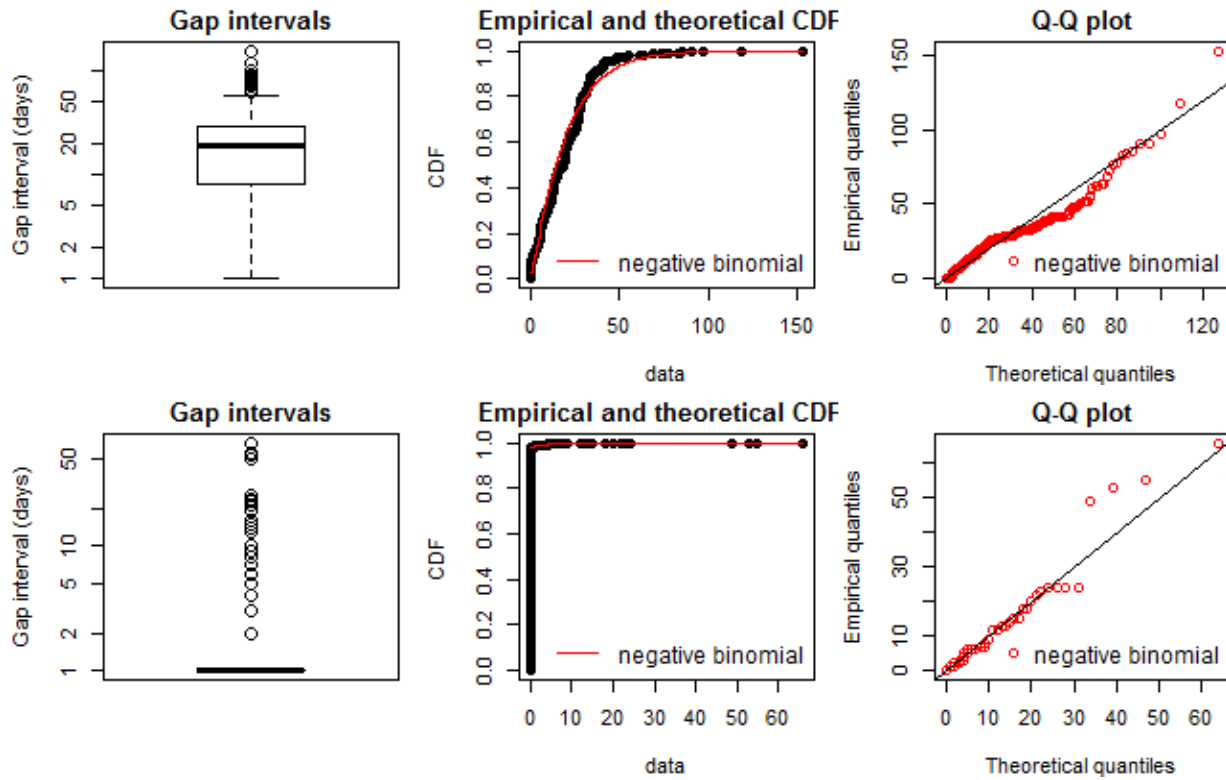
702 **Figure 1.** Synthetic time series with 200 time steps for three representative fractal scaling
 703 processes that correspond to white noise ($\beta = 0$), pink noise ($\beta = 1$), and Brown noise ($\beta = 2$).

704 The 1st row shows the simulated time series without any gap. The three rows below show the
 705 same time series as in the 1st row but with data gaps that were simulated using three different
 706 negative binomial (NB) distributions, that is, 2nd row: $\text{NB}(\lambda = 1, \mu = 1)$; 3rd row: $\text{NB}(\lambda = 1, \mu =$
 707 $14)$; 4th row: $\text{NB}(\lambda = 0.01, \mu = 1)$.



708

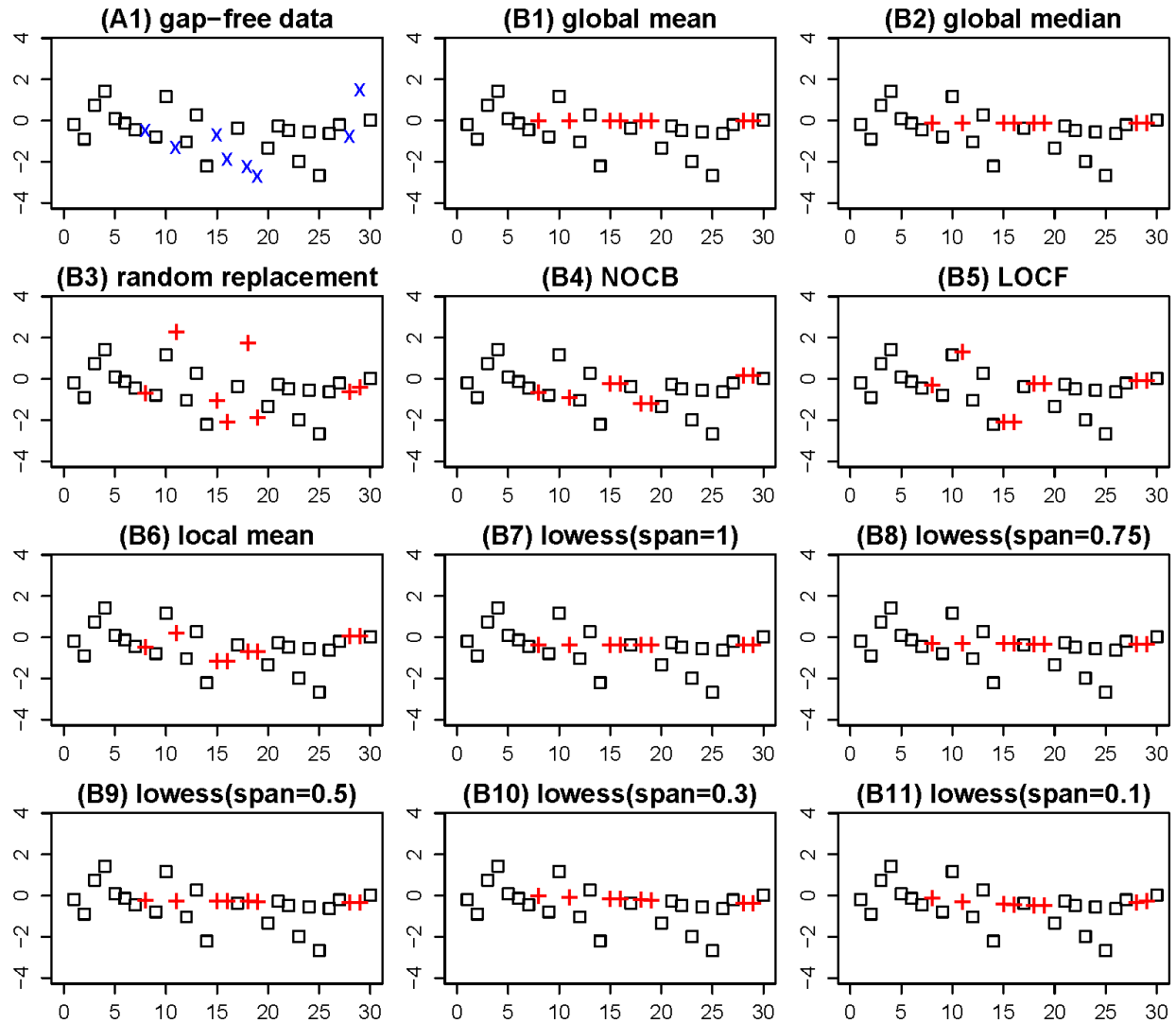
709 **Figure 2.** Examples of gap interval simulation using binomial distributions, NB (shape λ , mean
 710 μ). Simulation parameters: $L = 9125$ days, $\Delta t_{nominal} = 1$ day. The three panels show simulation
 711 with fixed (a) $\mu = 1$, (b) $\mu = 14$, and (c) $\lambda = 1$. Note that $\Delta t_{average}/\Delta t_{nominal} = \mu + 1$.



712

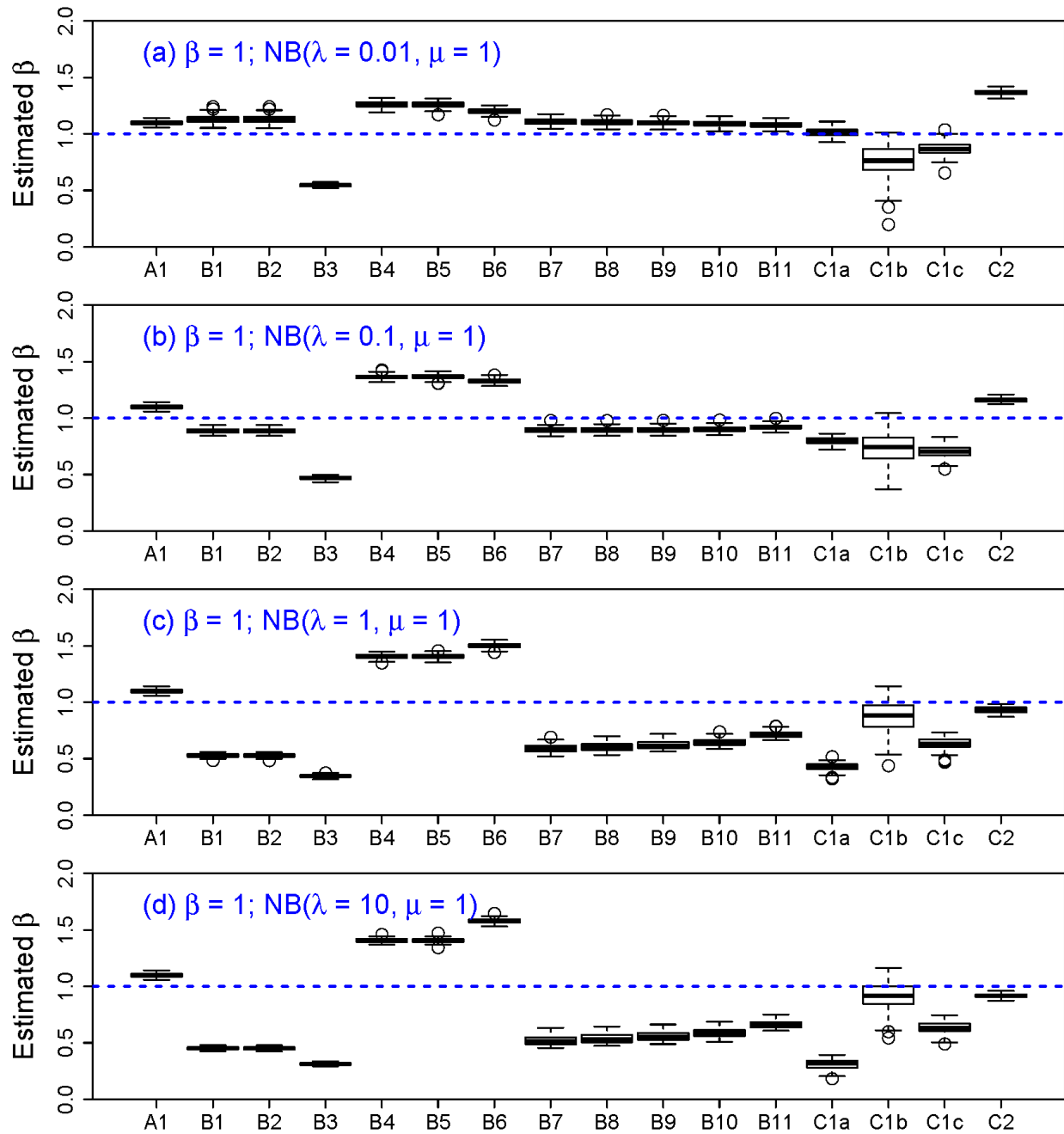
713

714 **Figure 3.** Examples of quantified sampling irregularity with negative binomial (NB)
 715 distributions: total nitrogen in Choptank River (top) and total phosphorus in Cuyahoga River
 716 (bottom). Theoretical CDF and quantiles are based on the fitted NB distributions. See **Table 1**
 717 for estimated mean and shape parameters.



718

719 **Figure 4.** Illustration of the interpolation methods for gap filling. The gap-free data (A1) was
 720 simulated with a series length of 500, with the first 30 data shown. (x: omitted data for gap filling;
 721 +: interpolated data; NOCB: next observation carried backward; LOCF: last observation carried
 722 forward; lowess: locally weighted scatterplot smoothing.)



723

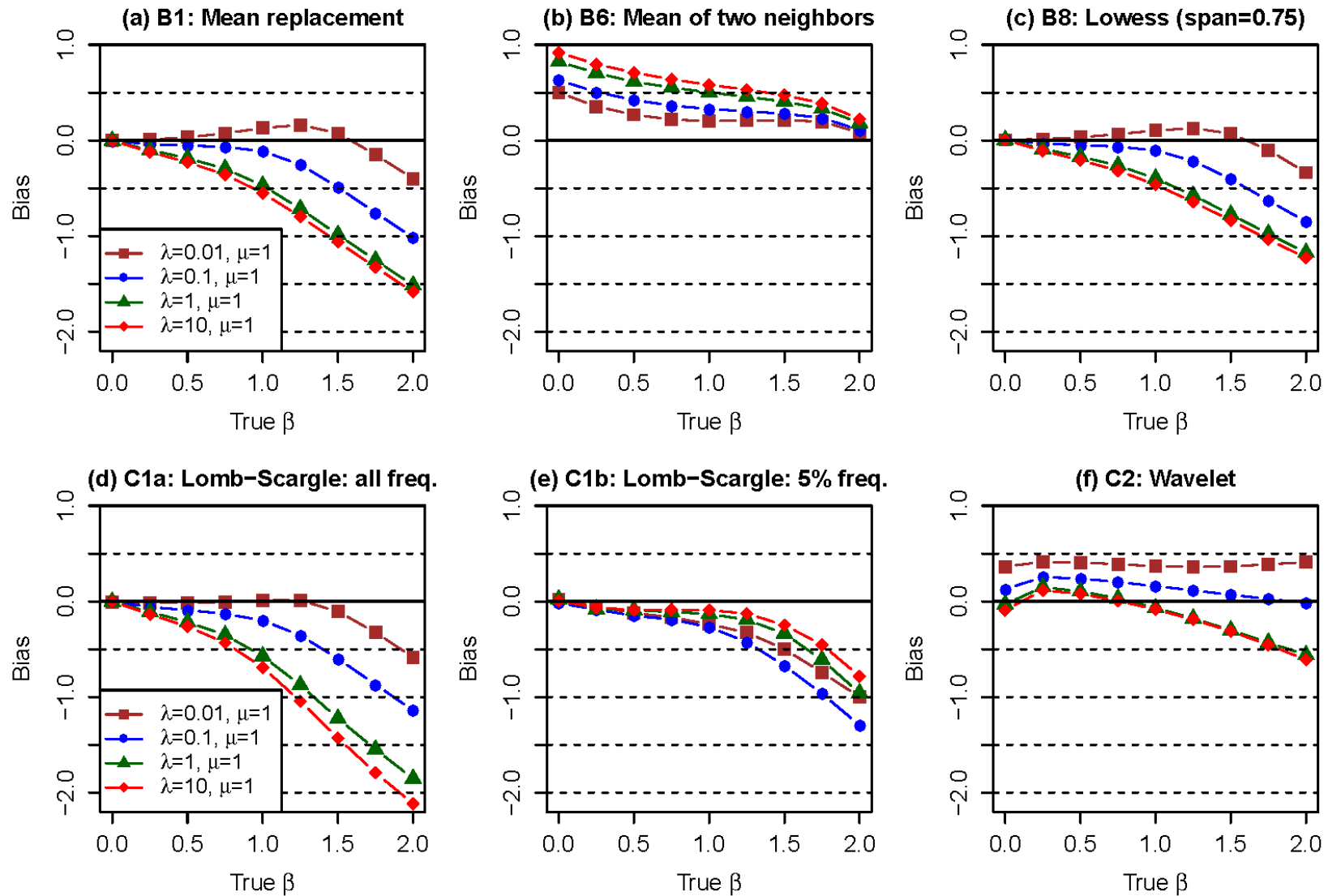
724

725

726

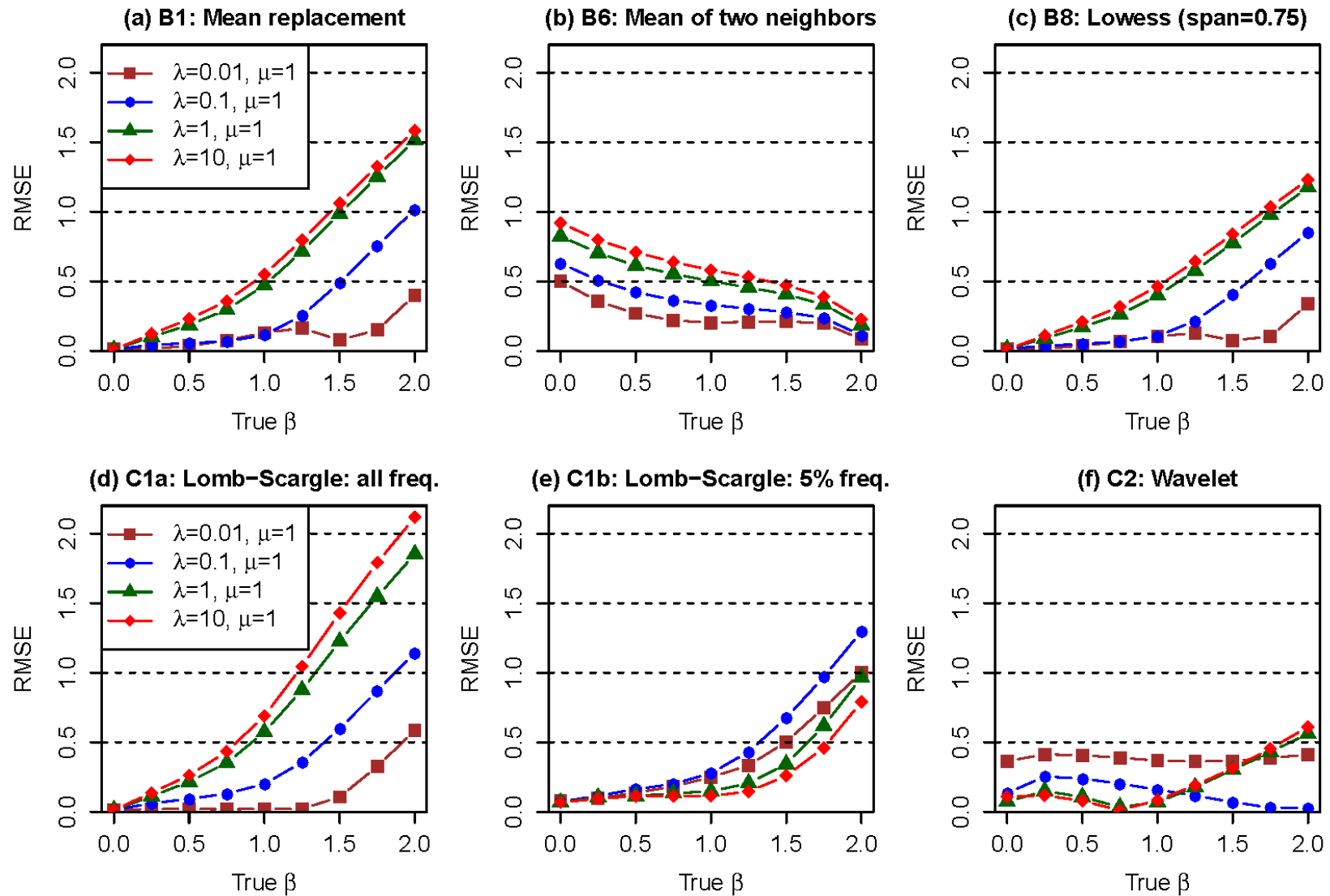
727

Figure 5. Comparison of bias in estimated spectral slope in irregular data that are simulated with prescribed $\beta = 1$ (100 replicates), series length of 9125, and gap intervals simulated with (a) NB ($\lambda = 0.01, \mu = 1$), (b) NB ($\lambda = 0.1, \mu = 1$), (c) NB ($\lambda = 1, \mu = 1$), and (d) NB ($\lambda = 10, \mu = 1$). The blue dashed lines indicate the true β value.



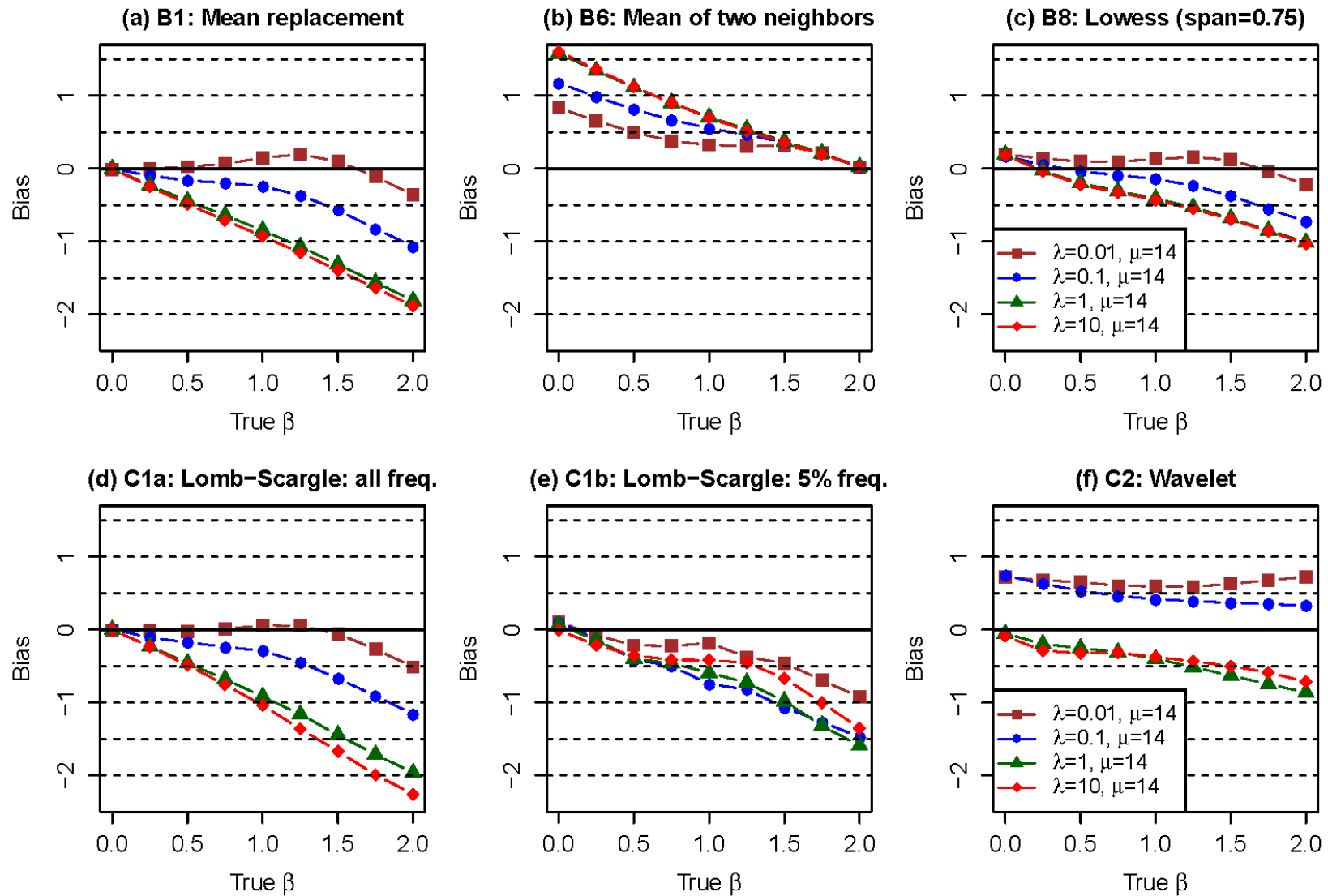
728

729 **Figure 6.** Comparison of bias in estimated spectral slope in irregular data that are simulated with varying prescribed β values (100
 730 replicates), series length of 9125, and mean gap interval of 2 (*i.e.*, $\mu = 1$).



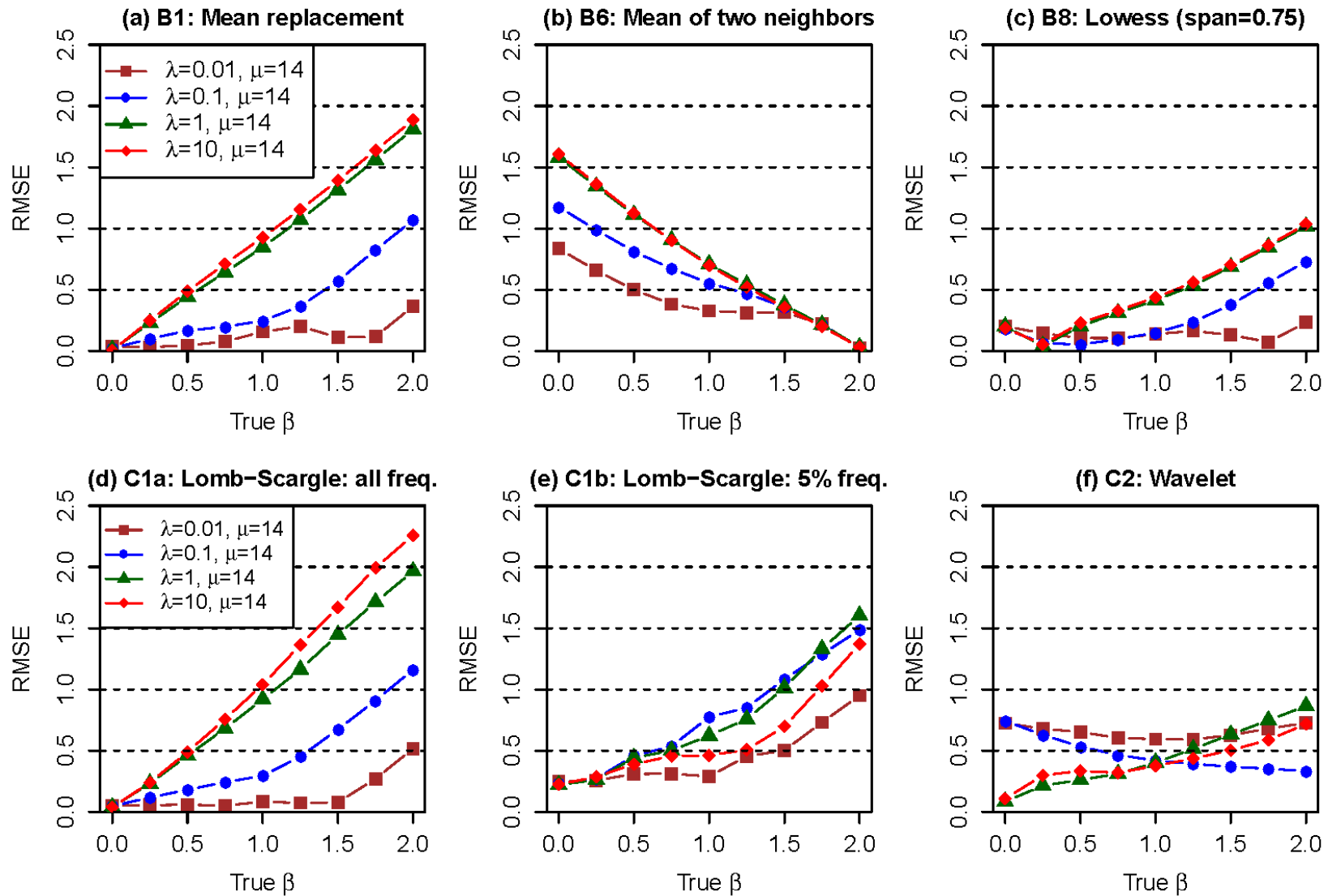
731

732 **Figure 7.** Comparison of root-mean-squared error (RMSE) in estimated spectral slope in irregular data that are simulated with varying
 733 prescribed β values (100 replicates), series length of 9125, and mean gap interval of 2 (*i.e.*, $\mu = 1$).



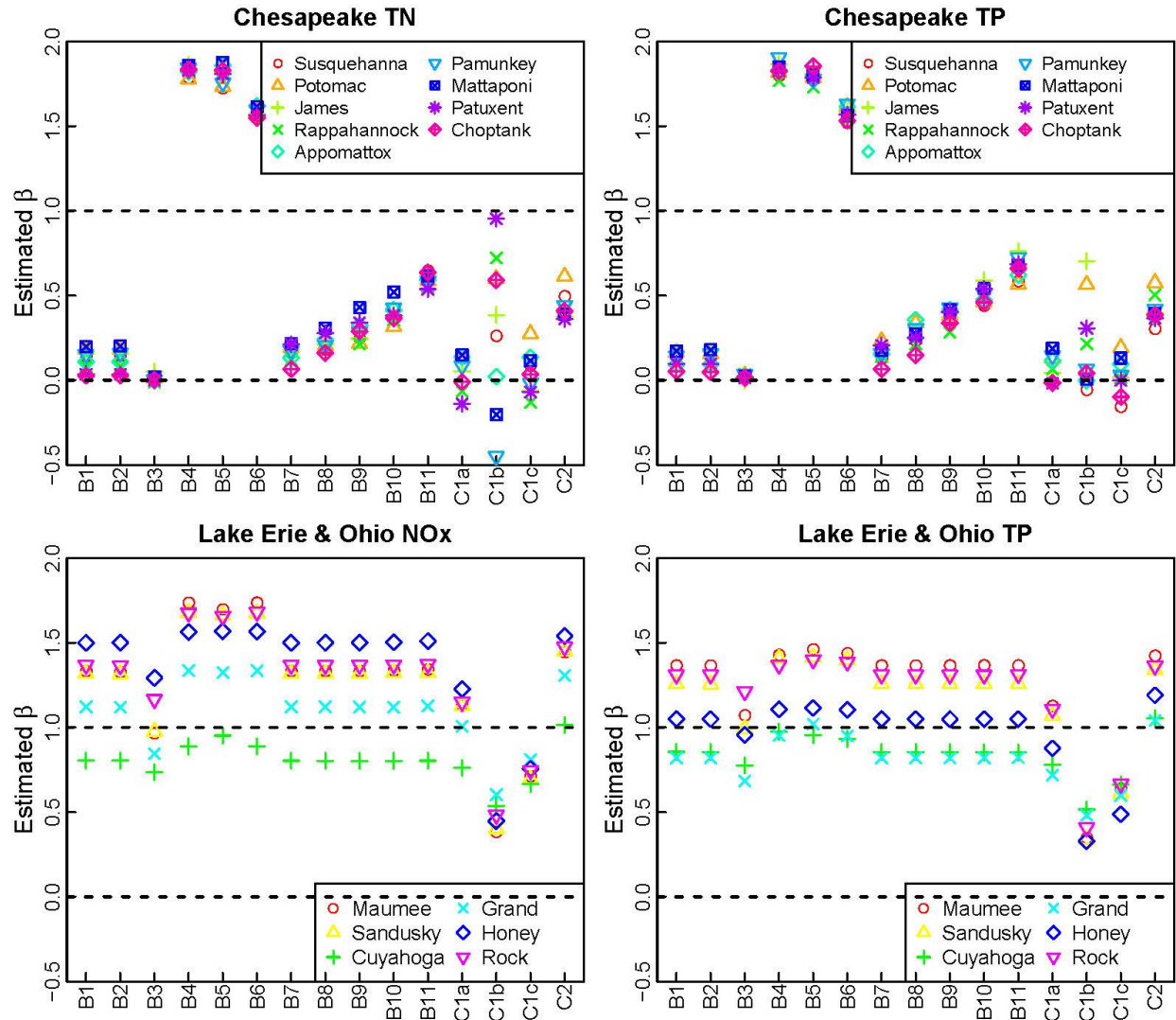
734

735 **Figure 8.** Comparison of bias in estimated spectral slope in irregular data that are simulated with varying prescribed β values (100
 736 replicates), series length of 9125, and mean gap interval of 15 (*i.e.*, $\mu = 14$).



737

738 **Figure 9.** Comparison of root-mean-squared error (RMSE) in estimated spectral slope in irregular data that are simulated with varying
 739 prescribed β values (100 replicates), series length of 9125, and mean gap interval of 15 (*i.e.*, $\mu = 14$).



740
 741 **Figure 10.** Quantification of spectral slope in real water-quality data from the two regional
 742 monitoring networks, as estimated using the set of examined methods. All estimations were
 743 performed on concentration residuals (in natural log concentration units) after accounting for
 744 effects of time, discharge, and season. The two dashed lines in each panel indicate white noise (β
 745 = 0) and pink (flicker) noise ($\beta = 1$), respectively. See **Table 1** for site and data details.